International Journal of Hydrogen Energy xxx (xxxx) xxx

Contents lists available at ScienceDirect

International Journal of Hydrogen Energy

journal homepage: www.elsevier.com/locate/he

A 4E analysis of different Fuel Cell mCHP configurations operating with different strategies in residential applications

P. Gabana [a,*], M. Reyes [a], F.V. Tinaut [b], R. Novella [b]

[a] Department of Energy and Fluid Mechanics Engineering, University of Valladolid, Paseo del Cauce 59, E-47011, Valladolid, Spain
[b] Institute CMT. Universitat Politècnica de València, Camino de Vera s/n, E-46022, Valencia, Spain

ARTICLE INFO

Handling Editor: Ibrahim Dincer

Keywords:
Fuel cell
Micro combined heat and power
Heat pump
Residential applications
Dynamic simulation
4E analysis

ABSTRACT

This study explores the viability, assessed in terms of primary energy, exergy, CO2 emissions, and economic benefits (4 E), associated with the integration of small-scale cogeneration systems (mCHP) utilizing proton exchange membrane fuel cells (PEMFC). The investigation is specifically oriented towards the residential sector. The model uses annual electrical and thermal demands as inputs. Parametric studies conducted through the modification of these values have been carried out. Dynamic demands are modelled using fixed consumption profiles to distribute the total annual demands.

Five configurations of CHP systems based on fuel cell technology (FC-mCHP) are analysed in this work. In the first configuration FC-mCHP uses hydrogen produced by an on-site steam methane reformer. In the second configuration FC-mCHP is fed with hydrogen coming from a centralized steam methane reformer. The third configuration is similar to the second configuration but with CO2 capture in the hydrogen generator. In the fourth configuration the FC-mCHP is supplied with hydrogen produced by an on-site electrolyser. In the fifth configuration the FC-mCHP utilizes hydrogen supplied from a centralized electrolyser. Each of these five configurations can be combined with a heat pump system, making a total of ten options.

In the FC-mCHP model, the electrical and thermal outputs are linked with the load of the system. The FC-mCHP load is set according to three operational strategies within each configuration: fulfil electricity demand, fulfil thermal demand, and fulfil both demands simultaneously. The FC-mCHP maximum electrical power serves as the sizing parameter. Additionally, the potential addition of a heat pump-based system is explored to increase thermal energy production. A conventional scenario is taken as a reference, in which electrical energy is taken from the grid, and thermal energy is supplied by a natural gas boiler.

The results show that there can be primary energy savings (between 20 and 60%) as well as CO2 emissions savings, with values depending on each configuration (up to 50% for the worst ones and up to 400% for the best ones) and the average operating conditions throughout the year. However, in general, all configurations lead to economic losses, compared with the reference conventional configuration. The results also indicate that the most effective strategy involves the FC-mCHP trying to satisfy both thermal and electrical demands. When the residential application is not connected to electric grid, the inclusion of a heat pump to the FC-mCHP yields relevant advantages, since additional thermal power can be generated in the heat pump, by converting part of electric power.

Nomenclature

Variables	Subscripts
CoP: Heat pump coefficient of performance. (–)	*A*: Annual average value
D: Demand (kW)	*c*: Heat pump cold source
E: Energy (kWh)	*D*: Demand

(continued on next column)

(*continued*)

g: Non ideality efficiency factor (–)	*el*: Electric
P: Power (kW)	*En*: Energy
T: Temperature (°C)	*Ex*: Exergy
Acronyms	*FC*: FC-mCHP system

(continued on next page)

This article is part of a special issue entitled: Hydrogen Utilization(Doranehgard) published in International Journal of Hydrogen Energy.

* Corresponding author.
E-mail addresses: pedro.gabana@uva.es (P. Gabana), miriam.reyes@uva.es (M. Reyes), ftinaut@mot.upv.es (F.V. Tinaut), rinoro@mot.upv.es (R. Novella).

https://doi.org/10.1016/j.ijhydene.2025.02.377
Received 27 September 2024; Received in revised form 19 February 2025; Accepted 23 February 2025
Available online 6 March 2025

(*continued*)

BoP: Balance of plant (−)	*G*: Imported from the electric grid
CHP: Combined heat and power (−)	*gl*: Global
FC-mCHP: Fuel cell micro combined heat and power system (−)	*h*: Heat pump hot sink
HPR: Heat to power ratio (−)	*HP*: Heat pump
SMR: Steam methane reforming	*H2*: Hydrogen supplied
Greek letters	*M*: Maximum
β: heat pump energy factor (−)	*Prim*: Primary (energy)
φ: fuel exergy factor (−)	*T*: Total
η: Efficiency (−)	*th*: Thermal
χ: Energy ratio (−)	

1. Introduction

In the current energy scenario marked by escalating costs of fossil fuels, there is a growing inclination towards the adoption of renewable energies and energy recovery systems to mitigate reliance on fossil fuels. However, the implementation of such systems requires comprehensive studies to ensure their effective utilization. Micro cogeneration or micro–Combined Heat and Power (mCHP) systems have emerged as promising solutions to reduce energy consumption and greenhouse gas emissions [1–3]. This is attributed to their capability to mitigate energy losses during transportation and decentralize electric power generation, offering potential reductions in both greenhouse gas emissions and energy costs within the residential sector [1].

Within mCHP systems, fuel cells (FC-mCHP) stand out as particularly promising technologies [2,4]. Their high electrical efficiency compared to other alternatives leads to low values of the heat to power ratios (*HPRs*) [5]. Moreover, fuel cells exhibit high reliability due to the lack of moving parts and an efficient operation at partial loads [3]. Consequently, numerous studies in the literature focus on the operation of FC-mCHP systems in residential contexts. These studies address control strategies [6–8], system sizing [9–11], current state and future trends [12], as well as performance within residential demands [11,13,14]. Some works explore the integration of FC-mCHP systems with other systems, such as underfloor heating [15], heat pumps [16,17], reversible absorption pumps [18–20], storage in water tanks or batteries [21] and photovoltaic systems [22]. The literature also features studies which use actual data from specific regions for comprehensive analyses [14,23,24] as well as comparing the performance of the same system working in different regions [20].

The dynamic operation of a fuel cell can be simulated to meet residential demands which some strategies to satisfy thermal demand, electrical demand, or both [20,25]. For example, Hawkes et al. [25] an economic comparison of the three strategies, considering three combined generation sources. Some authors consider also other possible strategies, but they have to include more facilities in the power generation system to store energy like electric batteries or hot water tanks [26]. The FC-mCHP electric efficiency can be calculated more accurately using a load profile. Arsalis [27] emphasizes the fundamental role of considering a load profile in the analysis, aligning with findings by Ref. [28] that underline the importance of the FC-mCHP electrical efficiency over results. Other works simulate only some specific representative days to avoid the computational effort of simulating a whole year [29].

The hydrogen used to feed fuel cells can be obtained from different sources. One of the most common methods to obtain hydrogen from fossil fuels is natural gas steam reforming [30]. Water splitting by electrolysis is another way to obtain hydrogen. Electrolysis can use electricity from renewable sources. Depending on the CO2 emissions produced in the generation of hydrogen, there is a colour code for the designation of hydrogen. Hydrogen obtained by steam reforming is designated grey hydrogen. If this process is coupled with a CO2 capture system, the hydrogen produced is designated blue hydrogen. Hydrogen produced from renewable energy sources can be considered green hydrogen [31]. Some works study the effect of using hydrogen from different sources in the FC-mCHP system [22], showing that the performance of the systems working with green hydrogen is worse than when working with natural gas as fuel.

The literature also presents numerous works focused on modelling fuel cell systems, ranging from predicting polarization curves [32–34] to modelling mass and heat flow within fuel cells for enhanced accuracy [35–37] or parameterising the stack overall performance [38]. Studies evaluating the suitability of fuel cells in residential applications typically assess primary energy savings [39], exergy analysis [17,40,41], CO2 emissions savings [42], and economic profitability [42]. It is important to contextualize studies on hydrogen technology against conventional technologies [25] and other mCHP systems like internal combustion engines [43], stirling and gas engines [25,44].

The objective of this works is to develop a comprehensive model to predict the PEM-based FC-mCHP performance (in terms of energies and efficiencies) in residential applications to identify new opportunities and trends. A dynamic Balance of Plant (BoP) model has been built, with the electrical demand estimated using real data from Ref. [45] and the thermal demand estimated using data from Ref. [46].

For this purpose, some FC-mCHP configurations are studied, which are aligned with those presented in a previous work [28]. In that work a sensitivity analysis was performed showing that the electrical efficiency of the fuel cell, the reduction in the cost of hydrogen and the improvement in the hydrogen production efficiency are parameters that have a decisive influence on global performance of the FC-mCHP in all configurations.

The novelty of the work lies in the number of configurations and FC-mCHP systems analysed and the method used to predict the electrical and thermal energy generated by the FC-mCHP system throughout all hours of a year, following the hourly demand profile specific of each day. With a scope further than that of [28], this paper explores a wider range of operating possibilities, with three control strategies (electrical demand, thermal demand or the most restrictive), and optionally including the combination with a heat pump subsystem to increase the thermal energy production. Energy and exergy analyses are included, with results presented in energy-exergy maps. The main results analysed are the comparison of the results of each configuration with a conventional situation in terms of primary energy, CO2 emissions and economic costs. This makes it possible to focus on operational modes and dynamic loads of the system.

2. Methodology

The model of the FC-mCHP is based on the one presented in Ref. [28], in which the overall efficiency of the FC-mCHP was defined as Eq. (1).

$$\eta_{gl,FC} = \eta_{el,FC} + \eta_{th,FC} = \frac{P_{el,FC}}{P_{H_2}} + \frac{P_{th,FC}}{P_{H_2}} < 1 \tag{1}$$

Were $\eta_{gl,FC}$ is the global efficiency, $\eta_{el,FC}$ is the electrical efficiency, $\eta_{th,FC}$ is the thermal efficiency, $P_{el,FC}$ is the electric power, $P_{th,FC}$ is the thermal power and P_{H_2} is the hydrogen power supplied to the FC-mCHP. The *HPR* of the FC-mCHP can be calculated as the ratio between the two efficiencies, as indicated in Eq. (2).

$$HPR_{FC} = \frac{\eta_{th,FC}}{\eta_{el,FC}} \tag{2}$$

In [28] $\eta_{el,FC}$ and $\eta_{th,FC}$ were configuration parameters fixed at a certain value. The results were generated based on the variation of the model inputs, which were the annual thermal and electrical demands, the mean electrical power and the number of operating hours of the FC-mCHP. Finally, a study was carried out analysing the results when $\eta_{el,FC}$ and $\eta_{th,FC}$ were independently modified (although maintaining the restriction that their sum must be limited below the value of 1). In the

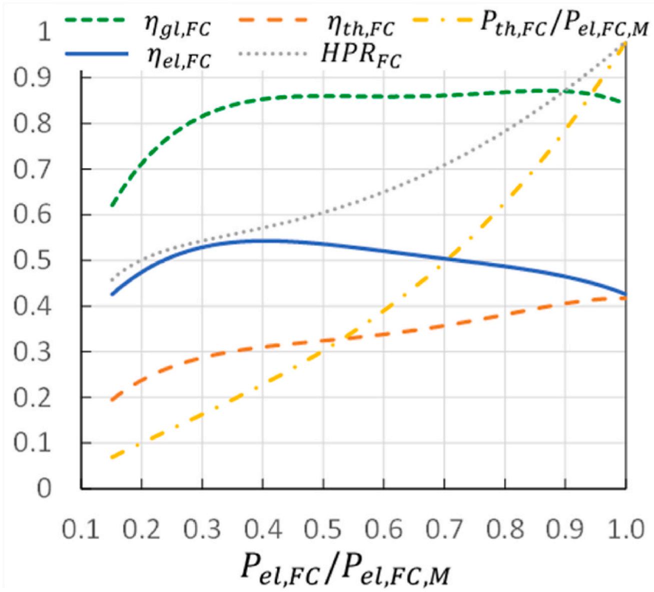

Fig. 1. FC-mCHP normalized performance curves.

present work $\eta_{el,FC}$ and $\eta_{th,FC}$ are calculated at each operating point (instead of being configuration parameters), depending on the actual values of energy demand and the *FC* characteristic performance plots.

2.1. Model description

This section includes first the FC-mCHP model used to calculate the electrical and thermal energies generated in each operating condition and second the estimation of the hourly profiles of the electric and thermal demands.

2.1.1. FC-mCHP model

The model considers both electricity and heat production, based on the values of the FC-mCHP characteristic curves FC-mCHP. Polynomial fits have been used to obtain $\eta_{el,FC}$ and $P_{th,FC}$ as a function of $P_{el,FC}$, used as main operating variable of the FC-mCHP.

The commercial balance of plant (BoP) data used are taken from Ref. [47], a PROTON MOTOR HyRange 25 (powered by PM400). Data have been normalized as follows. Powers ($P_{el,FC}$ and $P_{th,FC}$) have been normalized with respect to the maximum electrical power that can be supplied by the balance of plant ($P_{el,FC,M}$). Efficiency ($\eta_{el,FC}$) has been normalized with respect to the balance of plant maximum electrical efficiency ($\eta_{el,FC,M}$). The normalized electrical efficiency ($\eta_{el,FC}/\ \eta_{el,FC,M}$) as a function of the normalized electrical power ($P_{el,FC}/P_{el,FC,M}$) is then given by Eq. (3). The normalized thermal power ($P_{th,FC}/\ P_{el,FC,M}$) as a function of the normalized electrical power of the FC-mCHP ($P_{el,FC}/P_{el,FC,M}$) is given by Eq. (4).

$$\frac{\eta_{el,FC}}{\eta_{el,FC,M}} = -4.67\left(\frac{P_{el,FC}}{P_{el,FC,M}}\right)^4 + 12.44\left(\frac{P_{el,FC}}{P_{el,FC,M}}\right)^3 - 12.36\left(\frac{P_{el,FC}}{P_{el,FC,M}}\right)^2 + 5.14\left(\frac{P_{el,FC}}{P_{el,FC,M}}\right) + 0.26 \tag{3}$$

$$\frac{P_{th,FC}}{P_{el,FC,M}} = 0.87\left(\frac{P_{el,FC}}{P_{el,FC,M}}\right)^3 - 0.63\left(\frac{P_{el,FC}}{P_{el,FC,M}}\right)^2 + 0.78\left(\frac{P_{el,FC}}{P_{el,FC,M}}\right) - 0.04 \tag{4}$$

With Eq. (3) it is possible to calculate the electrical response of the FC-mCHP once a maximum electrical efficiency, $\eta_{el,FC,M}$, and a maximum electrical power, $P_{el,FC,M}$, are considered. Similarly, with Eq. (4) it is possible to calculate the thermal power of the FC-mCHP once a maximum electrical power, $P_{el,FC,M}$, is set as a model input. In the commercial balance of plant chosen as reference data [47], the maximum electrical efficiency was 53.8%, a value that has been kept in this work. The maximum electrical power $P_{el,FC,M}$ in the reference data was 36 kW. In the simulation work described later, the value of the maximum electrical power of the FC-mCHP is a free parameter, although it is assumed that the same type of correlations given by Eq. (3) and Eq. (4) are valid.

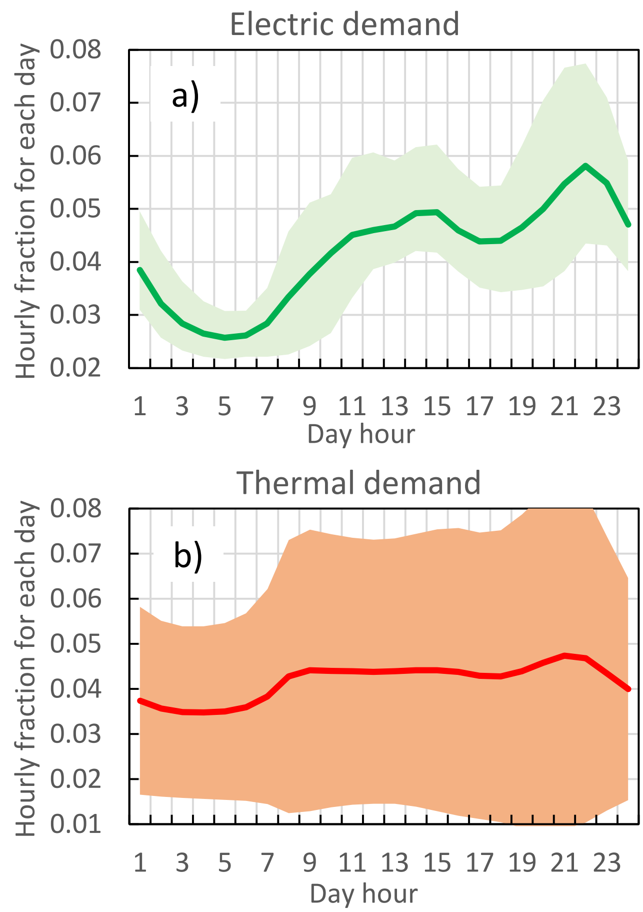

Fig. 2. Hourly demand profiles for each day of year. (a) Electrical demand profiles. (b) Thermal demand profiles. Shaded areas show dispersion due to seasonal variations while thick lines show annual averages.

Using Eq. (1), Eq. (2), Eq. (3) and Eq. (4), it is possible to plot the FC-mCHP characteristic curves as a function of the non-dimensionalised electric power, as shown in Fig. 1.

The characteristic curves are only plotted in the range 15–100% of $P_{el,FC,M}$, since this is the range in which experimental data are available. It can be observed in Fig. 1 that $\eta_{el,FC}$ has a variation of around 20% throughout its operating range (from 42% to 53.8%), with a maximum value for $P_{el,FC}/P_{el,FC,M} \sim 0.4$. In spite of the fact that $\eta_{th,FC}$, $P_{th,FC}$ and HPR_{FC} increase with $P_{el,FC}/P_{el,FC,M}$, the global efficiency $\eta_{gl,FC}$ remains roughly constant for values of the ratio $P_{el,FC}/P_{el,FC,M}$ bigger than 0.4. This is due to the fact that the drop in $\eta_{el,FC}$ is compensated with an increase in $\eta_{th,FC}$.

2.1.2. Electric and thermal demand estimation

The global inputs to the simulation of a given residential application are the total annual values of thermal ($D_{th,T}$) and electrical ($D_{el,T}$) demands. From them, an annual value of the heat to power ratio of the demand ($HPR_{D,A}$) can be used to characterize the application, as:

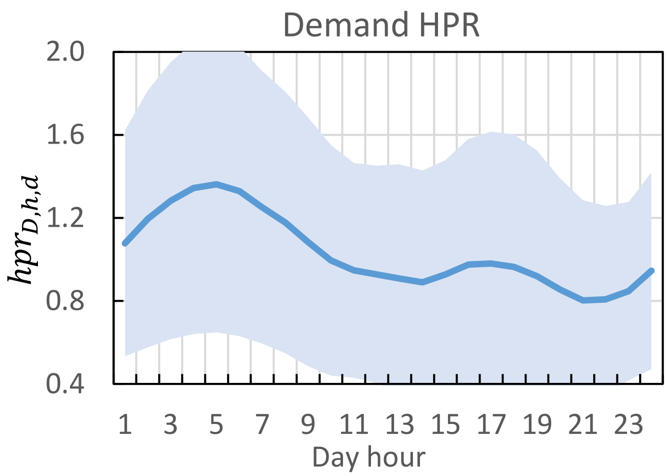

Fig. 3. Hourly heat to power ratio profiles for each day of year. Shaded area shows dispersion due to seasonal variations while the thick line shows the annual average.

$$HPR_{D,A} = \frac{D_{th,T}}{D_{el,T}} \tag{5}$$

Once the total annual values of the demands for a particular residential application are given, there is the need to distribute them throughout the hours and days of the year. This question has been addressed in different ways by other published works ([29,48]). In the present work, the demand profiles for each hour and day have been directly obtained from available published information, as described next.

2.1.2.1. Profiles of electrical demand. The hourly profiles of electricity demand for each day of year have been obtained (Fig. 2 (a)) from data available in Ref. [45] relative to Spain. The thick line shows the annual average (only as a reference), while the shaded region illustrates the seasonal dispersion. These profiles represent the fraction of electrical energy demanded in 1 h of a particular day. The electrical demand in each hour and day ($D_{el}(h,d)$, kWh/h) can be calculated as the total annual demand ($D_{el,T}$) times the non-dimensional profile.

2.1.2.2. Profiles of thermal demand. From the natural gas hourly demand records for Spain ([46]), the hourly profiles for each day of year of thermal energy demand for a single dwelling have been obtained, as represented in Fig. 2 (b). As for electricity, the thick line shows the annual average profile as a reference, while the shaded region represents the seasonal dispersion (stronger than for electricity). Again, the demand profiles correspond to the fraction of thermal energy demanded in each hour of a particular day of the year. Then the thermal demand in each hour and day ($D_{th}(h,d)$, kWh/h) can be calculated as the total annual demand ($D_{th,T}$) times the non-dimensional profile.

2.1.2.3. Profiles of heat to power ratio of the demand. Once the thermal and electrical hourly demands have been estimated, the associated profiles of heat to power ratio of the demand can be calculated, simply by the dividing the non-dimensional values of thermal and electrical profiles, as shown in Fig. 3.

It is important to note that, since the thermal and electrical profiles are already non-dimensional, the profile obtained as a ratio between them has been represented by lowercase letters ($hpr_{D,h,d}(h,d)$).

To summarize, the methodology used to account for the energy demands has the following steps.

- The starting point are the values of total annual electrical and thermal demands ($D_{el,T}$ and $D_{th,T}$), whose ratio is $HPR_{D,A}$.
- Electrical and thermal demand hourly profiles (one different for each day of the year) are considered and used to distribute the annual values $D_{el,T}$ and $D_{th,T}$, obtaining the values $D_{el}(h,d)$ y $D_{th}(h,d)$ in each hour and day of the full year.
- As a particular residential user is characterized by a given value of $HPR_{D,A}$ (depending on the relative importance of thermal demand versus electrical demand), different values of that ratio can be considered in the simulation to explore the possibilities of using the FC-mCHP + HP to cover the needs for a certain value of the nominal electric power (as described in a later section).

Table 1
Main differences of analysed configuration due to hydrogen production characteristics.

H2 Production	C1	C2	C3	C4	C5
Type	SMR	SMR	SMR	Electrolyser	Electrolyser
Location	On-site	Central	Central	On-site	Central
Heat recovery	Yes	No	No	Yes	No
CO2 emissions	Full	Full	CCS	Zero	Zero

2.2. FC-mCHP configurations

The configurations studied in this work initially are the same as in Ref. [28], which can be summarised as.

C0. Conventional systems for generation of electric power (with an energy mix) and heat (natural gas boiler). C0 is considered the reference for comparison of the performance of the other configurations.
C1. FC-mCHP fed with hydrogen produced by an on-site steam methane reformer (with heat recovery from hydrogen production, but without CO2 capture).
C2. FC-mCHP fed with hydrogen from a centralized steam methane reformer (without heat recovery nor CO2 capture).
C3. FC-mCHP fed with hydrogen from a centralized steam methane reformer with CO2 capture (without heat recovery).
C4. FC-mCHP fed with hydrogen produced by an on-site electrolyser (with heat recovery).
C5. FC-mCHP fed with hydrogen supplied from a centralized electrolyser (without heat recovery).

Configurations C1–C5 have been chosen because they cover three features: on-site hydrogen production (C1, C4) with associated heat recovery of the production versus centralised production (C2, C3, C5) without heat recovery; hydrogen production by steam reforming (C1, C2, C3) or by an electrolyser (C4, C5); and CO2 capture (C3) versus absence of capture (C1, C2, with no need in C4 and C5). In Table 1 the differences between C1–C5 configurations are presented. With the configurations chosen, there is the possibility to study the effects of using three types of hydrogen (grey, blue and green). Additionally, there is the possibility of adding a heat pump (HP) to the FC-mCHP system, leading to other additional five derived configurations (C1–C5 + HP).

2.3. Heat pump model

The heat pump has been modelled through its coefficient of performance (CoP_{HP}), which is the ratio between the electrical power consumed by the heat pump and the thermal power generated. The CoP_{HP} was calculated at each time of the year using Eq. (6) as in Ref. [49].

$$CoP_{HP}(t) = g_{HP} \cdot CoP_{Carnot} = g_{HP}\frac{T_h}{T_h - T_c(t)} \tag{6}$$

Where g_{HP} is a non-ideality factor, used to reduce the ideal coefficient of performance CoP_{Carnot}. The latter can be expressed in terms of T_h, the hot

Table 2
Configuration parameters used in the model [53–58,60–66].

Used in all configurations	Value	Units	Amortization (years)	Ref.
Electric power transmission efficiency	0.95			[53]
Cost of natural gas boiler	2000***	66.7 €/kW*30kW	15***	
Cost of electricity fixed term	16.34	€/kW-month*4kW		[54]
Cost of natural gas fixed term	9.52	€/month		[55]
Electricity cost	0.186	€/kWh		[54]
Natural gas cost	0.0403	€/kWh		[55]
CO2 emissions fee	85	€/ton$_{CO2}$		[56]
Conventional System C0	**Value**	**Units**		
Power generation efficiency	0.40			[57]
Natural gas boiler efficiency	0.93			[58]
Electricity CO2 emissions factor	260	g/kWh$_{el}$		[59]
Natural gas CO2 emissions factor	215	g/kWh$_{NG}$		[59]
Used in all FC-mCHP configurations	**Value**	**Units**	**Amortization (years)**	
Fuel cell cost	2000	€/kW$_{el}$	8**	[60]
Electricity selling price	0.09	€/kWh		[61]
C1	**Value**	**Units**	**Amortization (years)**	
Steam reformer efficiency	0.76			[59]
Onsite steam reformer thermal energy recovery fraction	0.83			[62]
Cost of onsite steam reformer	692	€/kW$_{NG}$	10***	[59]
C1 and C2	**Value**	**Units**		
CO2 emissions factor steam reforming	267	g/kWh$_{H2}$		[59]
C2	**Value**	**Units**		
Centralized steam reformer efficiency	0.76			[59]
Cost of grey H2	3.09	€/kg$_{H2}$		[63]
C3	**Value**	**Units**		
Centralized steam reformer with CCS efficiency	0.69			[59]
CO2 emissions factor of steam reforming with CCS	38.7	g/kWh$_{H2}$		[59]
Cost of blue H2	3.23	€/kg$_{H2}$		[63]
C4	**Value**	**Units**	**Amortization (years)**	
Onsite electrolyzer efficiency	0.64			[59]
Onsite electrolyzer thermal energy recovery fraction	0.76			[64]
Cost of onsite electrolyzer	1400	€/kW$_{H2}$	11***	[59]
C4 and C5	**Value**	**Units**		
Renewable energy efficiency	1.00			*
CO2 emissions factor of green H2	0	g/kWh$_{H2}$		[59]
Cost of renewable electricity	0.19	€/kWh		[65]
C5	**Value**	**Units**		
Centralized electrolyzer efficiency	0.64			[59]
Cost of electrolysis H2	6.96	€/kg$_{H2}$		[63]
Heat pump	**Value**	**Units**	**Amortization (years)**	
Heat pump cost	2100	300€/kW$_{th}$	20***	[66]

*In this work, the efficiency of renewable energy generation is (methodologically) assumed to be 100%, in accordance with the usual standard.
**The lifetime of the equipment has been used to estimate the amortization cost considering an annual use time of 4380 hours per year.
***Assumptions.

sink temperature, and T_c, the cold source temperature (usually the ambient air temperature). T_h is a model parameter, while T_c was obtained through data from a weather station located in Madrid [50]. In this work values of $g_{HP} = 0.5$ (the mean value considered in Ref. [49]) and $T_h = 45°C$ (a common value in domestic hot water consumption [51,52]) have been used.

3. Model utilization

3.1. FC-mCHP performance variables obtained with the model

The implemented model considers both electrical and thermal demands along all hours of a year, even if it they are very low compared with the assumed value of $P_{el,FC,M}$. During the simulation possible strategies are to set $P_{el,FC}$ trying to cover the electrical demand, the thermal demand or the most restrictive demand, with the restriction that $P_{el,FC}$ does not exceed the FC-mCHP operating limits. If the upper limit is exceeded ($P_{el,FC} > P_{el,FC,M}$), the operating point will be $P_{el,FC} = P_{el,FC,M}$. On the contrary, if the lower limit is exceeded ($P_{el,FC} < 0.15\,P_{el,FC,M}$), the operating point will be $P_{el,FC} = 0.15\,P_{el,FC,M}$. Thus, the FC-mCHP operates continuously throughout the year (in the range $0.15\,P_{el,FC,M}$ to $P_{el,FC,M}$).

Both demands are considered continuously variable functions, which means that at each time step they can take a different value. By changing the power demanded, the FC-mCHP tries to cover this power modifying $P_{el,FC}$ and consequently $\eta_{el,FC}$ and $\eta_{th,FC}$ will also change. The energy supplied and consumed by the FC-mCHP is obtained by time-integrating the powers. The equations used to obtain the electric energy supplied by the FC-mCHP ($E_{el,FC}$), the thermal energy supplied by the FC-mCHP ($E_{th,FC}$), and the hydrogen energy consumed by the FC-mCHP ($E_{H2,FC}$) are given in Eqs. (7)–(9).

$$E_{el,FC} = \int_0^t P_{el,FC}(t)\,dt \tag{7}$$

$$E_{th,FC} = \int_0^t P_{th,FC}(t)\,dt \tag{8}$$

$$E_{H2,FC} = \int_0^t P_{H2,FC}(t)\,dt = \int_0^t \frac{P_{el,FC}(t)}{\eta_{el,FC}(t)}\,dt \tag{9}$$

Primary energy savings have been estimated for the different configuration parameters and the values of Table 2. The efficiency and associated CO2 emissions of electricity production and hydrogen obtention of the specific pathway of each configuration are accounted for as presented in Ref. [28]. This provides the energy efficiency up to the hydrogen fed into the FC-mCHP. This energy efficiency from primary energy combined with the FC-mCHP efficiency leads to the complete transformation energy efficiency ($\eta_{En} < \eta_{gl,FC}$) from primary energy to electricity ($\eta_{el} \leq \eta_{el,FC}$) and thermal energy ($\eta_{th}$) produced by the FC-mCHP plus the heat pump in case it is implemented. The exergy efficiencies can be calculated from energy efficiencies as described in Appendix 1. CO2 emissions savings are strongly related to the primary energy savings, although each technology has a different CO2 emission factor. Similarly, economic savings have been estimated from configuration parameters and simulation results.

Due to the fact that the variation of the configuration parameters can change the results, a sensitivity analysis of the influence of changes in the model parameters was carried out in Ref. [28]. It was observed that the electrical performance of the fuel cell is the most influential parameter on the results.

3.2. FC-mCHP operation strategies

Three operating strategies have been considered. In the first one the FC-mCHP system works to meet the electrical demand D_{el}. In the second the FC-mCHP system works to cover the thermal demand D_{th}. In the third the FC-mCHP system works to try to meet both demands.

3.2.1. FC-mCHP system working to meet electric demand

In this situation, $P_{el,FC}$ is set to satisfy the electrical power demanded ($P_{el,D}$) at each time. Three situations can occur in each simulation time step:

- $0.15\,P_{el,FC,M} < P_{el,D} < P_{el,FC,M}$: in this situation, $P_{el,FC} = P_{el,D}$.
- $P_{el,D} < 0.15\,P_{el,FC,M}$: in this case, $P_{el,FC} = 0.15\,P_{el,FC,M}$, and the surplus energy ($0.15\,P_{el,FC,M} - P_{el,D}$) will be evacuated to the grid.
- $P_{el,D} > P_{el,FC,M}$: in this case, $P_{el,FC} = P_{el,FC,M}$, and the uncovered demand ($P_{el,D} - P_{el,FC,M}$) will be satisfied via grid connection.

In this control strategy the thermal power $P_{th,FC}$ is a result, with a value that depends on the operating point of the fuel cell (imposed by the value of the electric demand $P_{el,FC}$). If the thermal power $P_{th,FC}$ is higher than the value demanded ($P_{th,D}$), the excess ($P_{th,FC} - P_{th,D}$) is dissipated to the environment. On the other hand, if $P_{th,FC} < P_{th,D}$, the default demand ($P_{th,D} - P_{th,FC}$) is covered by means of a natural gas boiler. An explanatory flowchart of this strategy is shown in Appendix 2.

3.2.2. FC-mCHP system working to meet thermal demand

In this operating mode, the electric power $P_{el,FC}$ at each time step is chosen with the objective of generating enough thermal power $P_{th,FC}$ to cover the thermal demand $P_{th,D}(t)$. Thus, three situations can occur:

- The generated thermal power $P_{th,FC}$ equals the demand $P_{th,D}$, and the associated value $P_{el,FC}$ fits in the range between the minimum and the maximum electric power.
- If the thermal power demand leads to an operating point for which the electric power would fall below the minimum given by $P_{el,FC} = 0.15\,P_{el,FC,M}$, then the electric power of the fuel cell is set to that minimum. In addition, if $P_{th,D}$ is lower than the minimum $P_{th,FC}$, the excess of thermal energy is dissipated to the environment.
- Accordingly, if the thermal power demand leads to an operating point for which the electric power would be bigger than the maximum $P_{el,FC,M}$, then the FC-mCHP cannot fully satisfy the thermal demand $P_{th,D}$, and the uncovered demand must be covered via the natural gas boiler.

In this strategy, if $P_{el,FC} > P_{el,D}$, the power excess ($P_{el,FC} - P_{el,D}$) is fed-in into the grid, while if $P_{el,FC} < P_{el,D}$, the remaining demand ($P_{el,D} - P_{el,FC}$) is to be covered from the electrical grid.

3.2.3. FC-mCHP system working to meet the most limiting demand

This strategy attempts to satisfy at each time step the most limiting demand, electrical or thermal. For this purpose, every time step, the model evaluates which demand implies adopting a higher $P_{el,FC}$, i.e. a higher load for the FC system. Thus, $P_{el,FC}$ is changed to satisfy the demand that requires a higher $P_{el,FC}$. If satisfying the thermal demand requires a higher $P_{el,FC}$ than the needed to cover the electrical demand, the FC-mCHP system will work to cover the thermal demand. In the reverse situation, the FC-mCHP system will work to cover the electrical demand. An explanatory flow chart of this evaluation process is shown in Appendix 3.

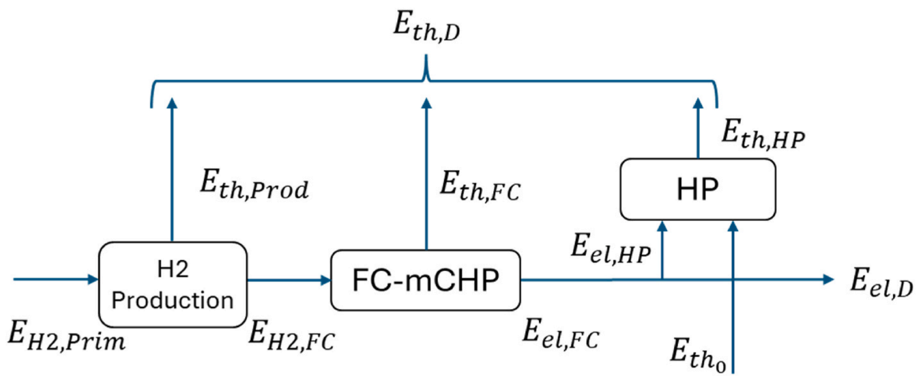

Fig. 4. Schematic of systems considered to satisfy the electrical and thermal demand.

3.2.4. FC-mCHP system combined with a heat pump

The assumption made in this extended configuration is that the FC-mCHP works in combination with a heat pump, so that the system is in a better situation to try to cover both D_{th} and D_{el}. This extended configuration has a great interest in many cases in which the heat to power ratio of the demand (HPR_D) is greater than the typical values of the fuel cell (HPR_{FC}). The heat pump then allows to convert electrical energy into thermal energy (with a CoP_{HP}) increasing the *HPR* of the energies produced. To calculate the operating value of the FC-mCHP in terms of electrical power $P_{el,FC}$, Eq. (10) is solved at each time step.

$$P_{th,D}(t) - P_{th,FC}(t) = P_{HP}(t)\; P_{HP}(t) = CoP_{HP}(t)\;\left(\left(P_{el,FC}(t) + P_{el,G}(t)\right) - P_{el,D}(t)\right) \tag{10}$$

where P_{HP} is the heat pump electricity power required to operate it to generate thermal power, and $P_{el,G}$ is the electric power imported from the grid (if needed).

When the HPR_D is lower than the HPR_{FC} it is not possible to match them, and the system will work to cover D_{el}. In this case, the excess of thermal power generated by the system will be dissipated to the environment.

4. Results analysis and discussion

The simulation time is extended to all 8760 h of a full year by using an in-house Matlab code. Two sets of results have been obtained, the first one analyses the differences between different operation strategies that the FC-mCHP can follow and the second one studies the feasibility of the combination of the FC-mCHP and a heat pump. In all cases, the results for the five configurations C1–C5 are presented simultaneously. The analysed results are primary energy savings, energy and exergy

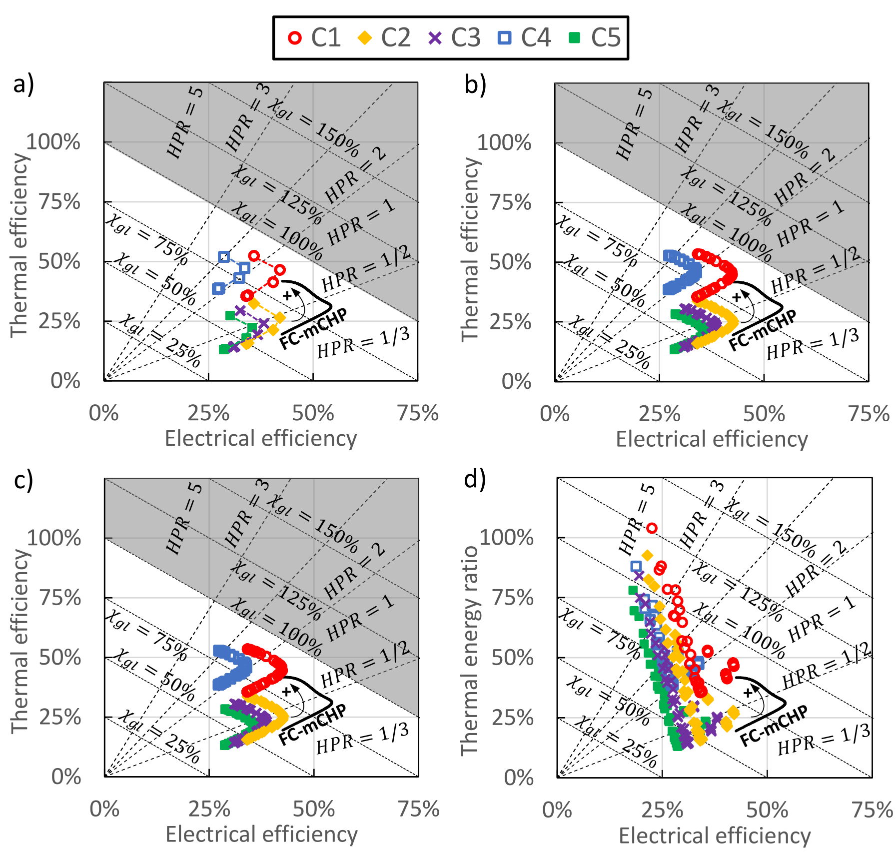

Fig. 5. η_{el}-η_{th} coordinate plane of C1–C5 from primary energy to final FC-mCHP production. FC-mCHP system working to satisfy: (a) the electric demand, (b) the thermal demand, (c) the highest demand, (d) the highest demand plus combination with a heat pump. Grey shaded areas in (a), (b) and (c) are non-allowed points.

efficiencies, CO2 emissions savings and economic savings.

In all simulations presented the annual electrical demand $D_{el,T}$ is set at 4380 kWhel. This value is equivalent to a constant demand of 0.5 kW and is in accordance with the results of Kilpatrick R et al. [67]. On the other hand, the annual thermal demand $D_{th,T}$ is set to have values of $HPR_{D,A}$ of 0, 0.5, 0.75, 1, 1.5, 2, 2.5, 3, 4, 5, 6 and 8. Additionally, the values of $P_{el,FC,M}$ considered are 0.5, 1, 2, 4, 6 and 10 kWel.

4.1. Energy analysis from primary energy

The combination of operating conditions of the FC-mCHP throughout the year provides the instantaneous values of electric and thermal power in each hour of the year. The integration of powers (according to Eq. (10)) allows obtaining the values of the energy demanded by the FC-mCHP, as well as the energies generated by it, with the possibility of combining with a heat pump. As said, the heat pump efficiently uses part of generated electricity to pump heat taken from environment at a temperature compatible with thermal demand. Moreover, if the processes of generating the hydrogen needed to feed the FC-mCHP are considered, the primary energy consumption is given. Since these processes can generate rejected heat, part of it can be also used to satisfy the thermal demand, although only with on-site production (C1 and C4 configurations). The relevant terms can be seen in Fig. 4.

As a result of the simulations performed combining the values of $HPR_{D,A}$ and $P_{el,FC,M}$, the efficiencies (η_{el} and η_{th}) of hydrogen production from primary energy to energy generated by FC-mCHP have been plotted on a η_{th}-η_{el} coordinate plane (Fig. 5) as in Refs. [1,68].

The annual values of the electrical and thermal efficiencies of the FC-mCHP alone are calculated using Eqs. (11) and (12):

$$\eta_{el,FC} = \frac{E_{el,FC}}{E_{H2,FC}} \tag{11}$$

$$\eta_{th,FC} = \frac{E_{th,FC}}{E_{H2,FC}} \tag{12}$$

Where $E_{H2,FC}$ is the energy associated with the hydrogen used to feed the FC-mCHP during the year. These efficiencies correspond to the FC performance characteristics and thus are independent of the hydrogen production processes. In the following figures, in a plane thermal efficiency-electrical efficiency, a single black line represents the relationship between them.

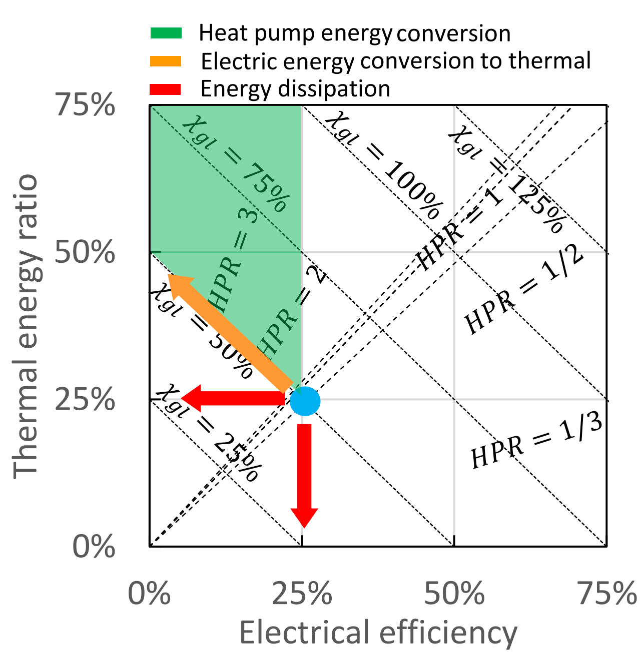

Fig. 6. Schematic diagram of displacement possibilities within the coordinate plane η_{el}-χ_{th}.

Similarly, accounting for the hydrogen production processes plus the possible combination with a heat pump leads to similar expressions as Eqs. (11) and (12), but considering the amount of primary energy required to generate the hydrogen that feeds the FC-mCHP Eqs. (13) and (14) respectively:

$$\eta_{el,FC+HP} = \frac{E_{el,FC}}{E_{H2,Prim}} \tag{13}$$

$$\chi_{th,FC+HP} = \frac{E_{th,FC} + E_{th,HP}}{E_{H2,Prim}} \tag{14}$$

In the case of thermal energy, the term χ appearing in Eq. (14) is called energy ratio instead of thermal efficiency since the term corresponding to the heat E_{th_0} taken from environment is not considered in the denominator of the expression and under certain conditions the energy ratio χ can be higher than unity.

Similarly, the annual global energy ratio of the FC-mCHP + HP from primary energy is calculated using Eq. (15):

$$\chi_{gl,FC+HP} = \frac{E_{el,D} + E_{th,FC} + E_{th,HP}}{E_{H2,Prim}} = \eta_{el,FC+HP}[1 + HPR_{FC} + \beta_{HP}(CoP - 1)] \tag{15}$$

With $\eta_{el,FC+HP}$ given by Eq. (13), i.e. defined in terms of primary energy. The parameter β_{HP} quantifies the fraction of electrical energy produced by the FC-mCHP that is used to drive the heat pump (see Appendix 1 for full details).

With the definition of these efficiencies and ratios including the hydrogen production processes, each configuration (C1 to C5, plus the heat pump) has different numerical values, as can be seen in the following figures of results.

Strictly speaking, Eq. (15) is valid only for configurations in which the rejected heat of hydrogen production is not used (C2, C3 and C5). For the other two configurations (C1 and C4) in which that heat is used to satisfy part of the thermal demand, the numerical value of the global efficiency can be easily computed by just simply adding the recovery term ($E_{th,Prod}$) in the numerator, but it is very difficult to obtain an explicit expression.

As for $\chi_{th,FC+HP}$, with the proposed definition of $\chi_{gl,FC+HP}$, since the term corresponding to the heat taken from environment is not introduced in the denominator of Eqs. (14) and (15), in some cases the global energy ratio can reach values higher than unity. Despite this been counterintuitive, it has been decided to keep this definition since it strongly reveals the benefits of increasing thermal energy ratio (and by extension, global energy ratio) by introducing a heat pump.

Fig. 5(a) and (b) and (c) show the results of the FC-mCHP annual efficiencies (Eqs. (13) and (14)) from primary energy of the configurations C1 to C5, operating with three different control strategies, i.e. following (a) electric demand, (b) thermal demand and (c) highest demand. Fig. 5 (d) shows the results for the combined system FC-mCHP + HP, for the case of following the highest demand. The results for each configuration are denoted with differentiated colour markers. To help interpreting the results, auxiliary lines of constant values of energy ratio χ_{gl} and heat to power ratio HPR are included. Grey shaded areas are non-allowed operating conditions of the FC-mCHP (limited by the restriction that the global energy efficiency must be lower than unity). However, not a similar restriction is applied to the combined FC-mCHP + HP system, due to the environment term.

For comparison, the FC-mCHP efficiencies (Eqs. (11) and (12)) from the supplied hydrogen energy to FC-mCHP generated energies have also been plotted with a black line (the arrow shows the sense of increasing power). In general, it can be seen that electrical efficiency of the

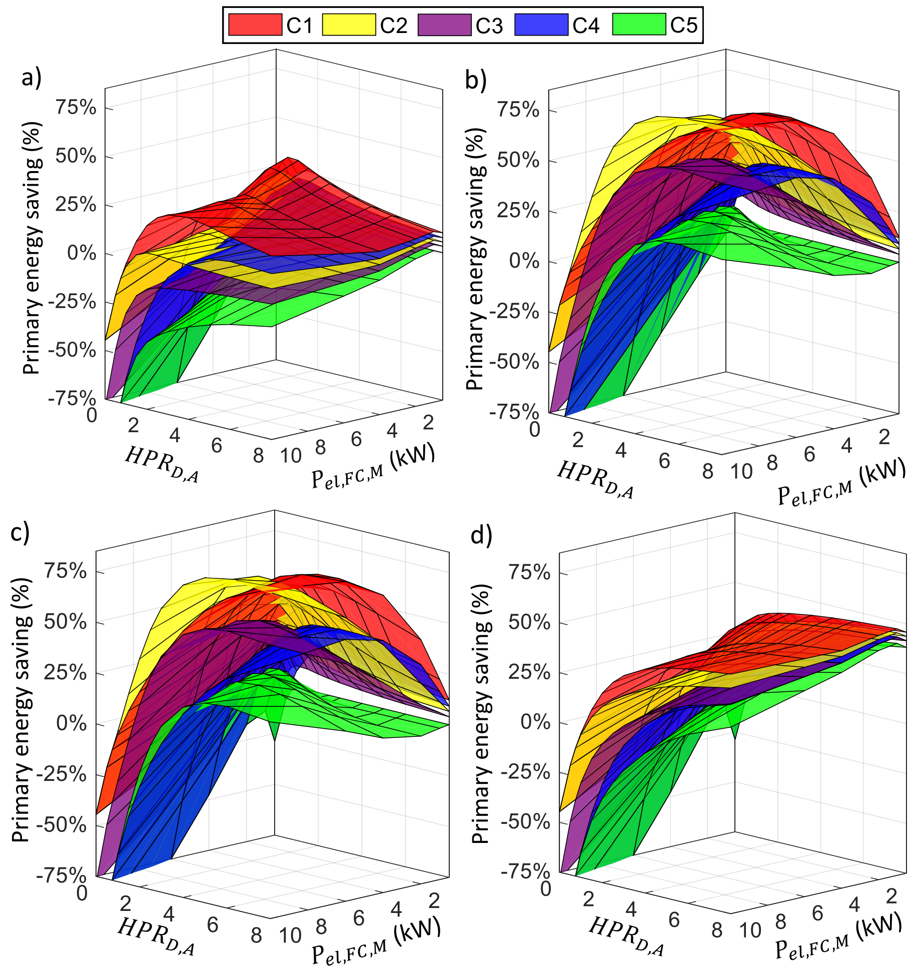

Fig. 7. Primary energy savings of C1–C5 considering energy fed-in electricity to the grid. FC-mCHP system working to satisfy: (a) the electric demand, (b) the thermal demand, (c) the highest demand, (d) the highest demand plus combination with a heat pump.

production system plus the FC-mCHP (Eqs. (13)–(15)) is always reduced compared to the values of the FC alone. On the other hand, thermal efficiency of the whole system can be increased over that of the FC alone, although only when the heat rejected from hydrogen production is used (C1 and C4). In any case, the *HPR* of the FC-mCHP in any of the configurations is bounded between the lines $HPR = 1/3$ and $HPR = 2.5$ (approx.).

The energy ratio χ_{gl} is strongly increased when a heat pump is included, with the counterpart of reducing electric efficiency. As a consequence of this, the *HPR* increases, moving operating points to the left and higher in the plane (limited by an $HPR = 5$).

It can also be seen in Fig. 5 (a) there are less operation points than in Fig. 5(b) and (c). This is because, when the control strategy is to meet the electricity demand (a), modifying the *HPR* of the demand does not change the system operating point.

Fig. 5 (d) shows that introducing a heat pump is equivalent to having an additional degree of freedom, making it possible to move the *HPR* of the power generation by decreasing η_{el} and increasing χ_{th}. This explains why there are more possible operation points for this system. The higher the CoP_{HP}, the greater the increase of χ_{th} achieved with the same reduction of η_{el}. Since $\chi_{gl} = \chi_{th} + \eta_{el}$, the higher the CoP_{HP} the greater the possibility of increasing χ_{gl}. However, CoP_{HP} depends on T_H and T_C (Eq. (6), with the higher T_H the lower the CoP_{HP}).

Fig. 6 shows the different possibilities to move the system operating point within the coordinate plane χ_{th}-η_{el}. For instance, the red arrow moving downwards illustrates the case when thermal energy is dissipated, while the red arrow moving to the left corresponds to the case in which electric energy is fed into the grid (and then not used in the application). On the other hand, it is also possible to directly transform electric energy into heat (by a resistance heater, orange arrow), with the overall efficiency (from primary energy to final energy) remaining constant. The green region is where it is possible to move the operating points by using a heat pump, depending on the value of the heat pump CoP_{HP} (which in turn determines the ratio χ_{th}/η_{el}).

It is possible to move to almost all positions of the coordinate plane χ_{th}-η_{el} that are to the left of the vertical line given by the value of η_{el}. However, even with addition of the heat pump, it is not possible to move to the right of that vertical line. The other limitation of the movement of the operating point within the coordinate plane χ_{th}-η_{el} is the electrical-to-thermal energy conversion technology. Ideally, the technology used should start from a point that allows the movement to the largest possible number of points of the coordinate plane χ_{th}-η_{el}, with the maximum achievable electric efficiency η_{el}. In this way, it would be possible to regulate the *HPR* of the generation system and move to higher global energy ratios, χ_{gl}.

Fig. 7 shows the primary energy savings of all configurations (C1–C5) referred to C0, as a function of the maximum electrical power of FC ($P_{el,FC,M} = [0.5, 10]\ kW$) and the annual average value of heat-to-power ratio ($HPR_{D,A} = [0, 8]$). The results have been plotted as surfaces. Each subfigure in Fig. 7 shows the results when the strategy is covering: (a) electric demand, (b) thermal demand, (c) both demands and (d) both demands plus combination with a heat pump.

In general, it can be seen that for all configurations there are regions, characterized by low values of the demand annual heat to power ratio

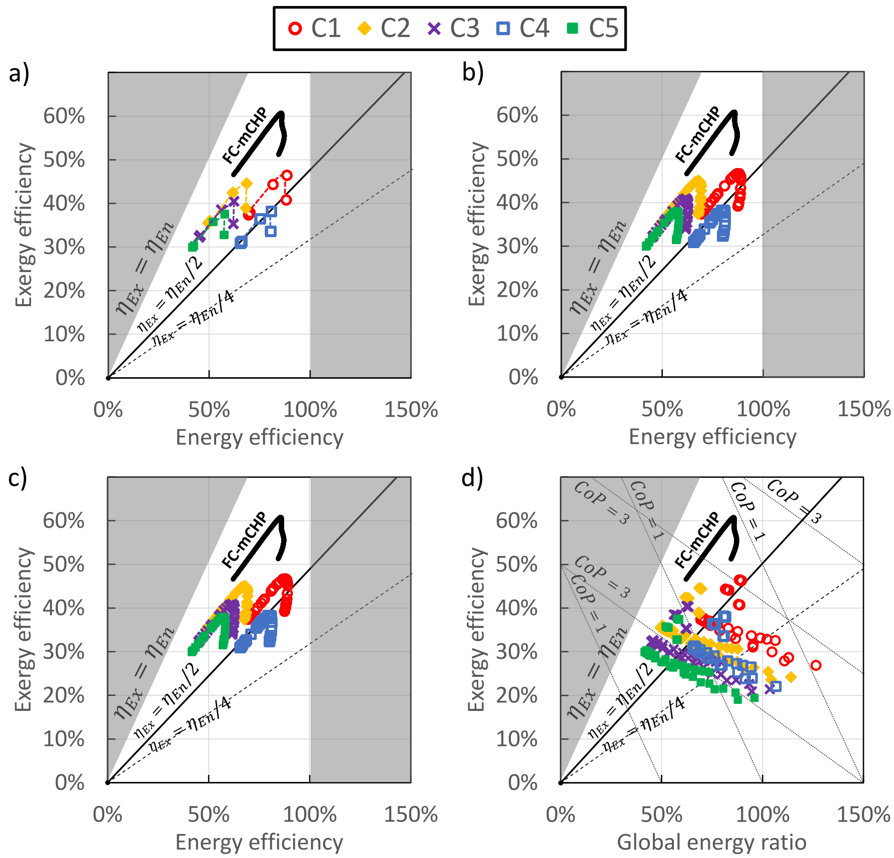

Fig. 8. η_{En}-η_{Ex} coordinate plane of C1–C5 from energy generation to final FC-mCHP production. FC-mCHP system working to satisfy: (a) the electric demand, (b) the thermal demand, (c) the highest demand, (d) the highest demand plus combination with a heat pump. Grey shaded areas are non-possible points.

$HPR_{D,A}$, in which primary energy savings are negative (i.e., losses), while for high values of $HPR_{D,A}$, primary energy savings are achieved. It can also be observed in Fig. 7 that there are two trends. First, configurations with no heat recovery of hydrogen production (C2, C3 and C5) have surfaces that are quasi-parallel and do not intersect each other. C5 always performs worse than C3, that in turn always performs worse than C2, because hydrogen generation efficiency in C5 is lower than in C3 which in turn is lower than in C2. Secondly, configuration with on-site hydrogen production (C1 and C4) that allow recovery of heat rejected during that process, show similar trends, as the differences between them lie in the efficiency of the hydrogen generation system and the efficiency of the energy transport system (Table 2). The hydrogen generation system is more efficient in C1 (although using a fossil resource) than in C4 (that uses renewable energy), so primary energy savings always are higher in C1 than in C4.

Fig. 7 (a) shows that in all configurations (C1–C5) the primary energy savings tend to 0 as $HPR_{D,A}$ increases, this is because $D_{el,T}$ is constant while $D_{th,T}$ increases with $HPR_{D,A}$. Since the system works to satisfy D_{el}, as D_{th} increases the total energy covered by the FC-mCHP is relatively lower. Furthermore, as $D_{el,T}$ is not changed during the simulations, the highest primary energy savings are achieved with $P_{el,FC,M} = 1kW$ in all configurations C1–C5. Although in Fig. 7 (a) FC-mCHP works to satisfy D_{el}, the systems that make use of the heat rejected from the hydrogen production process (C1 and C4) can save more energy when $HPR_{D,A} > 1$, with a maximum for a value close to 2. When $HPR_{D,A} < 1$, there is an excess of $E_{th,FC}$ that is dissipated to the environment. In configurations without thermal utilization in the hydrogen production (C2, C3 and C5), the highest primary energy savings are achieved when $HPR_{D,A}$ is close to 0.5.

When the FC-mCHP works to satisfy the thermal demand D_{th} (Fig. 7 (b)), it can be observed for all configurations C1–C5 that with a $HPR_{D,A}$ of 0 there are negative primary energy savings, since the FC-mCHP system works in the lower limit ($P_{el,FC} = 0.15\ P_{el,FC,M}$). When $HPR_{D,A}$ is increased, maximum primary energy savings are achieved increasing $P_{el,FC,M}$. With the same value of $HPR_{D,A}$, C1 and C4 require less $P_{el,FC,M}$ than C2, C3 and C5 to obtain the highest primary energy savings.

When the FC-mCHP works to meet the highest demand (Fig. 7 (c)), the results are a combination of the results of Fig. 7 (a) and 7 (b). With low $HPR_{D,A}$ values the results resemble those in Fig. 7 (a), while for high $HPR_{D,A}$ values the results are close to those in Fig. 7 (b), with a transition value of $HPR_{D,A}$ that depends on the configuration. In configurations without thermal utilization in the hydrogen production (C2, C3 and C5), the value of $HPR_{D,A}$ is around 0.5, while in configurations with thermal utilization in the hydrogen production (C1 and C4) the value of $HPR_{D,A}$ is around 2.

Finally, Fig. 7 (d) shows the primary energy savings of C1–C5 configurations of the FC-mCHP combined with a heat pump, again as a function of $P_{el,FC,M}$ and $HPR_{D,A}$. In this case, all configurations C1–C5 have similar trends, since the different between them come from the different hydrogen production efficiency. In general, primary energy savings are slightly higher when the maximum power of the FC system $P_{el,FC,M}$ reduces. However, the influence of $P_{el,FC,M}$ on the results is much lower than that of $HPR_{D,A}$.The bigger the weight of the heat pump in the amount of thermal energy generated, the bigger the energy savings. In general, the higher the value of $HPR_{D,A}$ and the lower the value of $P_{el,FC,M}$, the higher energy savings.

4.2. Exergy analysis from primary energy

Mean annual exergy efficiencies of the FC-mCHP alone are calculated using Eqs. (16) and (17) (more details can be found in Appendix 1):

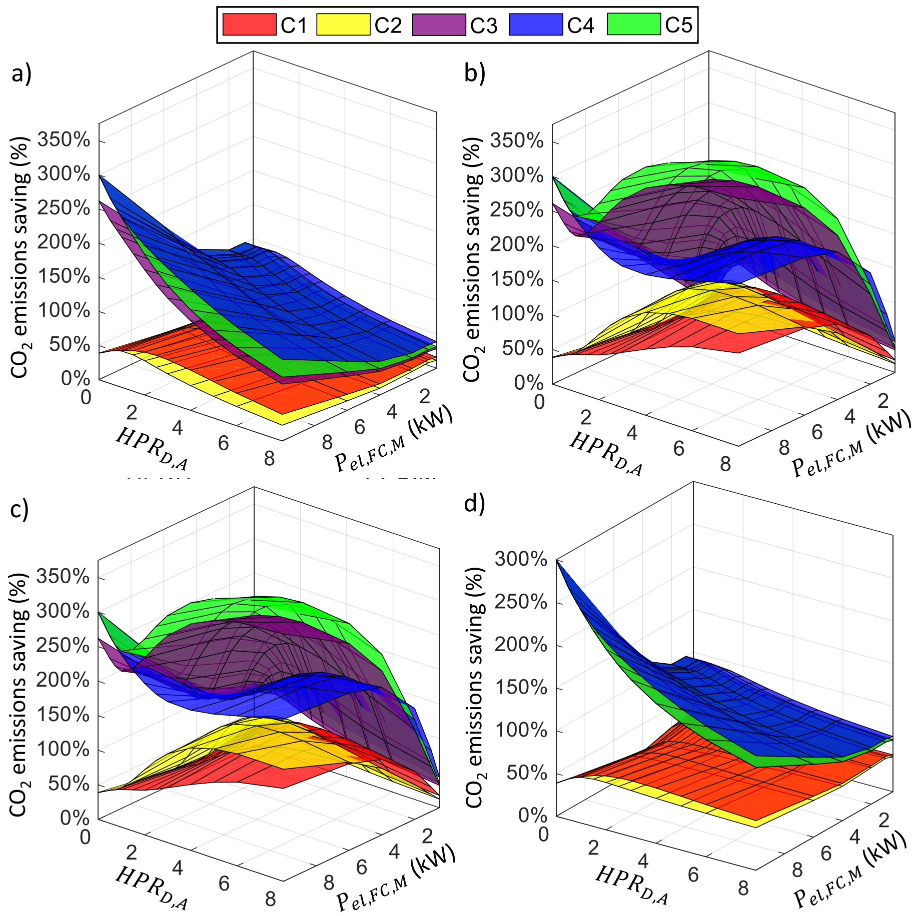

Fig. 9. CO2 emissions savings of C1–C5. FC-mCHP system working to satisfy: (a) the electric demand, (b) the thermal demand, (c) the highest demand, (d) the highest demand plus combination with a heat pump.

$$\eta_{Ex,el,FC} = \frac{Ex_{el,FC}}{Ex_{H2,FC}} = \frac{1}{\varphi_{H2}} \eta_{el,FC} \tag{16}$$

$$\eta_{Ex,th,FC} = \frac{Ex(E_{th,FC})}{Ex_{H2,FC}} = \frac{1}{\varphi_{H2}} \eta_{th,FC} \left(1 - \frac{T_0}{T_{th,FC}}\right) \tag{17}$$

The mean annual exergy efficiency of electricity in the FC-mCHP is equal the energy efficiency of electricity, except for the fuel exergy factor for hydrogen φ_{H2} (that is very close to 1, exactly 0.985 [69]). On the other hand, the mean annual thermal exergy efficiency is calculated as the thermal energy efficiency multiplied by the Carnot factor corresponding to the hot temperature sink and the inverse of the factor φ_{H2}.

The mean annual global exergy efficiency of the FC-mCHP + HP is calculated using Eq. (18) (details in Appendix 1):

$$\begin{aligned} \eta_{Ex,FC+HP} &= \frac{E_{el,D} + E_{th,FC}\left(1 - \frac{T_0}{T_{th,FC}}\right) + E_{th,HP}\left(1 - \frac{T_0}{T_{th,HP}}\right)}{\varphi_{H2} \bullet E_{H2,Prim}} \\ &= \frac{\eta_{el,FC+HP}}{\varphi_{H2}} \left[1 + HPR_{FC}\left(1 - \frac{T_0}{T_{th,FC}}\right) + \beta_{HP} \bullet \left(CoP\left(1 - \frac{T_0}{T_{th,HP}}\right) - 1\right)\right] \end{aligned} \tag{18}$$

Where $\eta_{el,FC+HP}$ is given by Eq. (13), to account for the hydrogen production phase.

As in the case of the energy efficiency (Eq. (15)), the expression of exergy efficiency Eq. (18) is strictly only valid for configurations C2, C3 and C5 in which no heat is recovered from hydrogen production. For configurations C1 and C4, the global exergy efficiency can be also numerically computed by considering the exergy of the thermal recovery term ($Ex_{th,Prod}$) in the numerator, but it is too complex to write an explicit expression. Concerning the thermal energy term taken from the environment by the heat pump, its exergy is zero so there is no need to consider it so the expression Eq. (18) is strictly less than 1.

Fig. 8 shows the coordinate plane η_{Ex}-η_{En} where the simulation results have been positioned. This figure shows the efficiencies from primary energy to final energy. Grey shaded areas represent non allowed operating points, similar for the three cases of operation of the FC alone. When a heat pump is added, the restriction of the energy efficiency lower than unity disappears, since the energy of the heat taken from environment in not explicitly consider in the definition of energy efficiency. However, the exergy of this heat is zero (due to its temperature) and for that reason, there is no need to include it in the exergy efficiency.

Note in Fig. 8(a) and (b) and (c) that for all configurations C1–C5 and regardless of the operating strategy, the ratio η_{Ex}/η_{En} is always bounded between 0.3 and 0.7 (with a mean value of 0.5). The exergy efficiencies of configurations with hydrogen production by reforming (C1 and C2) are higher than those of the configurations with hydrogen production by electrolysis (C4 and C5). This is because the reforming efficiency (0.76) considered (Table 2) is higher than the electrolyser efficiency (0.64). In case of configuration C3, hydrogen is also produced by reforming, but the CO2 capture reduces the efficiency to an intermediate value of 0.69.

When a heat pump is added (Fig. 8 (d)), the energy ratio always increases, although the exergy efficiency decreases. The higher the value of CoP_{HP} the more the χ_{gl} is increased with an associated reduction of the η_{Ex}.

In an off-grid generation system, it is useful to introduce a heat pump that adapts the *HPR* of the generation to the demand *HPR*. However, in a grid-connected system, it could be more interesting to export electrical energy to the grid, avoiding the exergy destruction in the heat pump.

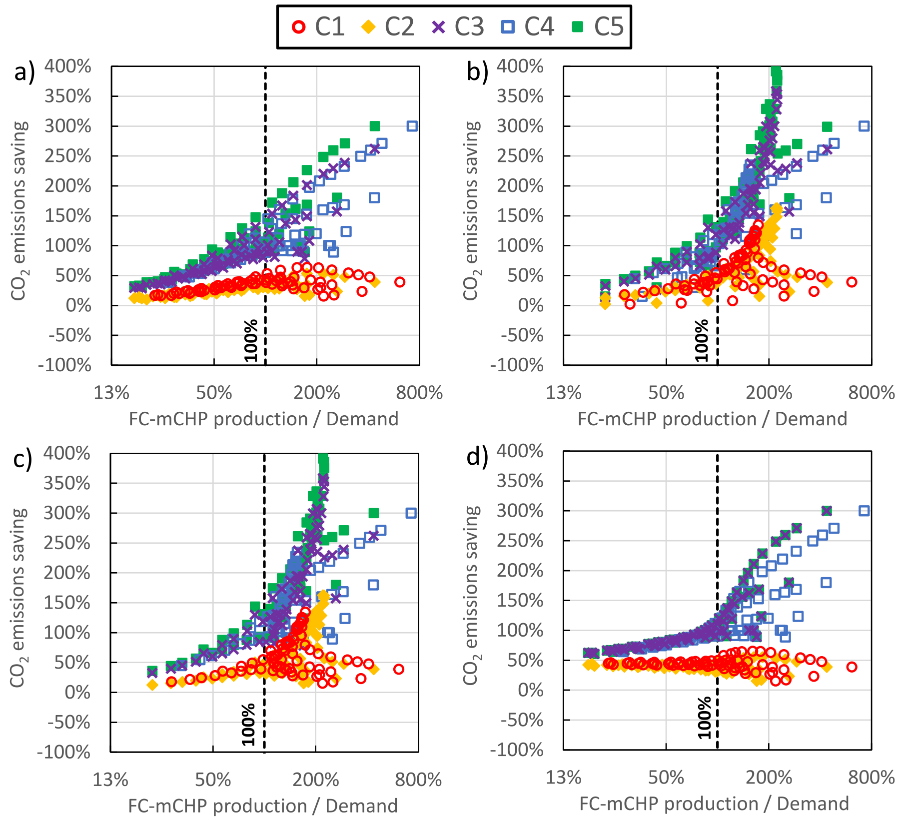

Fig. 10. Distribution of CO2 emissions savings as a function of the demand covered by the FC-mCHP for C1–C5. FC-mCHP system working to satisfy: (a) the electric demand, (b) the thermal demand, (c) the highest demand, (d) the highest demand plus combination with a heat pump.

4.3. CO2 emissions savings considering primary energy consumption

CO2 emissions savings have been calculated for the annual operation of all configurations C1–C5 using as a reference configuration C0. The values have been calculated using the same approach as in Ref. [28]. The methodology consists in calculating the energy consumption by source with each configuration and multiplying by the CO2 emissions factor [59]. For all configurations, when consuming energy from the conventional grid, the CO2 emissions factors for electricity and natural gas are used (Table 2). Also, CO2 emissions factor of green H2 is used in C4 and C5, CO2 emissions factor of H2 obtained from steam reforming is used in C1 and C2, and CO2 emissions factor of H2 obtained from steam reforming with CCS is used in C3.

Fig. 9 shows the CO2 emission savings of C1–C5 as a function of $P_{el,FC,M}$ and $HPR_{D,A}$ when the strategy is to meet: (a) electric demand, (b) thermal demand, (c) both demands and (d) both demands plus a combination with a heat pump.

In general, there are CO2 emission savings, although the savings strongly depend on the configuration type and the operating point (given by the power and heat to power ratio of the demand). Thus, configurations with hydrogen obtained by SMR (C1 and C2) present low saving values as they have CO2 emission factors of the order of C0. If CO2 capture in included in the reforming process (C3), the trends are closer to the configurations with hydrogen obtained by electrolysis with renewable energy (C4 and C5). In some operating points, C4 (on-site electrolyser with heat recovery) performs better than C5 (centralised electrolyser). In addition, there can be CO2 emission savings greater than 100% due to the consideration of CO2 emissions savings of the electric energy exported to the grid.

In Fig. 9 (a) CO2 emissions savings tend to 0 since demand increases when increasing $HPR_{D,A}$ without varying the FC-mCHP operating point. In this situation, for C3–C5, the CO2 emission savings grow with $P_{el,FC,M}$ and decreases with increasing $HPR_{D,A}$. In addition, with low $HPR_{D,A}$, not much natural gas is consumed in the boiler, which improves CO2 emission savings.

In Fig. 9 (b) CO2 emissions savings increase with $HPR_{D,A}$ due to the increase of electrical power exported to the grid. In addition, with high $HPR_{D,A}$ and low $P_{el,FC,M}$ the FC-mCHP system operates at full load, and any demand above the maximum thermal output of the FC-mCHP is met by the natural gas boiler, which reduces CO2 emissions savings. Therefore, increasing $P_{el,FC,M}$ also increases CO2 emissions savings.

In Fig. 9 (c), similar results to the best of the two previous strategies are obtained at each $HPR_{D,A}$ and $P_{el,FC,M}$. In addition, it is remarkable that the first strategy (Fig. 9 (a)) obtains better results with low $HPR_{D,A}$ and low $P_{el,FC,M}$, while the second strategy (Fig. 9 (b)) works better for high $HPR_{D,A}$ values and high $P_{el,FC,M}$.values.

Fig. 9 (d) shows CO2 emission savings results for C1–C5 when FC-mCHP is combined with a heat pump as a function of $P_{el,FC,M}$ and $HPR_{D,A}$. The results obtained are very similar to Fig. 9 (a). CO2 emission savings higher than 100% can only be achieved when electrical energy is fed back to the grid. The strategy only allows dumping electrical energy to the grid when $HPR_{D,A}$ is low and $P_{el,FC,M}$ high. If electrical energy is taken from the grid to run the heat pump because $D_{el} > P_{el,FC,M}$ the CO2 emission savings are due to thermal energy savings.

To explore more in depth the results of CO2 emissions savings for each operating mode, they have been plotted as a function of the fraction of global demand covered by the FC-mCHP (Fig. 10). As can be seen in Fig. 10, there are points at which the FC-mCHP generates more energy than the demanded (percentages higher than 100% in the abscissas axis). This is due to the possibility of exporting electricity to the grid and also dissipating thermal energy to the environment. When electric energy is exported to the grid, this represents a primary energy saving, and therefore the corresponding CO2 emissions savings can be computed. However, when thermal energy is dissipated to the environment, there is

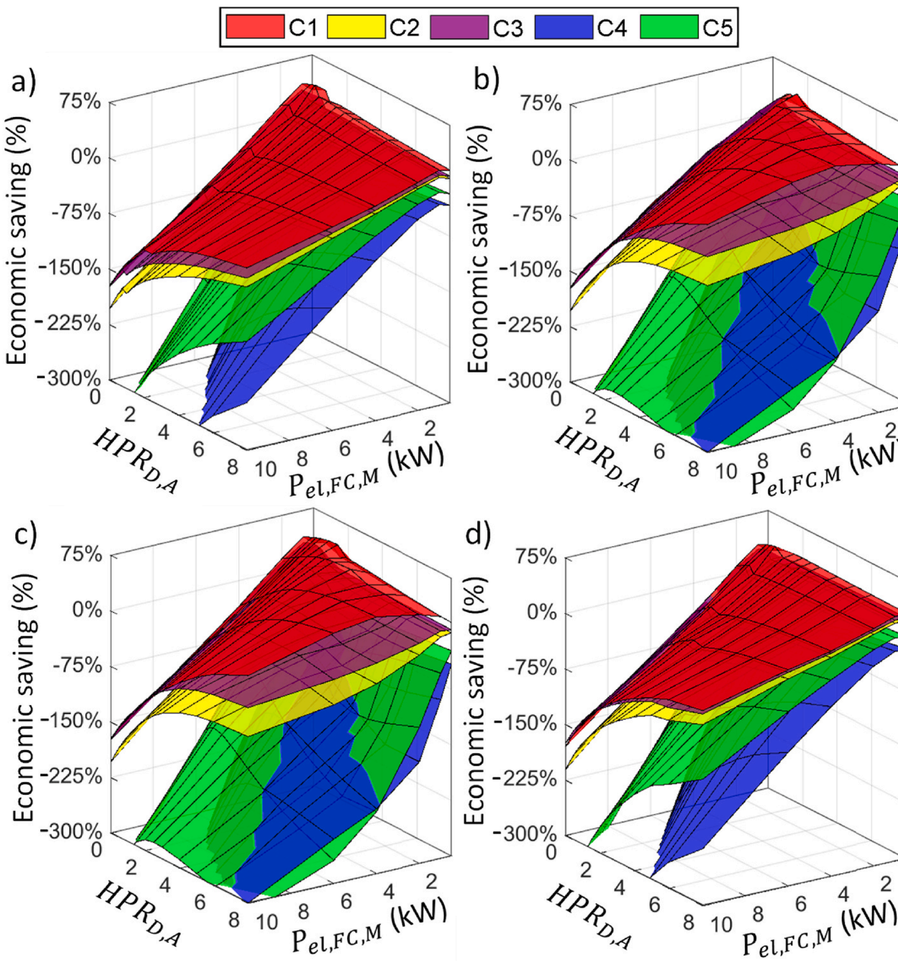

Fig. 11. Economic savings of C1–C5 considering energy fed back to the grid. FC-mCHP system working to satisfy: (a) the electric demand, (b) the thermal demand, (c) the highest demand, (d) the highest demand plus combination with a heat pump.

no CO2 emissions benefit. Fig. 10 shows that for configurations C3, C4 and C5, the CO2 emission savings are higher when the energy supplied by the FC-mCHP is higher.

4.4. Economic analysis from primary energy

The economic analysis of the energy production using the FC-mCHP system has been performed, including the investment costs and operative costs (Table 2) of the different configurations, and compared with the reference configuration C0. The comparison provides positive savings in some cases, but also negative savings (losses) in other cases.

Fig. 11 shows the annual economic savings results of configurations C1–C5 as a function of $P_{el,FC,M}$ and $HPR_{D,A}$, when the strategy is to meet: (a) electric demand, (b) thermal demand, (c) both demands and (d) both demands plus combination with a heat pump. In the model when a certain system is not used in some specific operating conditions, for instance the natural gas boiler, its cost is not accounted for the calculations. This can cause sharp changes in the results.

All configurations follow similar trends, ranging from negative savings (losses) in most of the operating conditions to positive savings. For a given configuration, the most influencing parameter is the nominal electric power of the FC-mCHP. Positive savings are achieved for small values of the nominal power. Configurations with hydrogen production by steam reforming (C1, C2 and C3) are the most cost-effective configurations, for the assumed cost of natural gas. C2 and C3 only differ in hydrogen cost and CO2 emissions factors. Configurations with hydrogen production by electrolysis (C4 and C5) economically perform worse, with C4 being slightly worse than C5 since the on-site electrolyser leads to a higher equivalent hydrogen cost.

Fig. 11 (d) shows economic savings results for C1–C5 for the combination FC-mCHP + HP, as a function of $P_{el,FC,M}$ and $HPR_{D,A}$. Trends obtained are very similar to Fig. 11 (a). In this case there are no abrupt changes in the results surfaces, since the natural gas boiler is not needed in any configuration. In case of not being able to export electricity to the grid, the combination of a heat pump-based with the FC-mCHP can provide significant advantages.

As a final comment, when comparing the CO2 savings (Fig. 9) with the economic savings (Fig. 11), in general opposite trends can be observed. This means that CO2 savings can be achieved, but with higher costs than with the reference configuration.

5. Conclusions

In this work, a model has been developed to calculate the response of the FC-mCHP system along a full year, adapting its operating point to the varying electrical and thermal demands. Algebraic relationships of electric efficiency and thermal power of the FC-mCHP have been used to model the system. Five configurations (C1–C5) have been considered, with the same FC-mCHP system but with different alternatives for hydrogen production (SMR, electrolysis, on-site, centralized, with and without recovery of rejected heat, with and without CO2 capture). Additionally, there is the possibility for each configuration to combine it with a heat pump (FC-mCHP + HP) to allow generating more thermal energy, increasing the heat to power ratio. Three operating strategies have been considered: covering the electrical demand, the thermal demand, and the highest demand.

The main trends observed from the analysis of results (energy efficiency, exergy efficiency, CO2 emissions savings, economic analysis) of the operating conditions of the system throughout a full year are.

- When the hydrogen production is accounted for, the electrical efficiency from primary energy is reduced compared to the FC efficiency. However, the thermal efficiency can be increased in configurations (C1 and C4) in which there is recovery of heat rejected in the hydrogen production.
- The introduction of a heat pump strongly increases the thermal efficiency (up to 90% in some points) at the expense of the electrical efficiency. It also extends the possibility to satisfy thermal demands with higher heat to power ratios (up to 5).
- Similar trends appear for exergy efficiency from primary energy. As a reference, exergy efficiency is about a half of energy efficiency. Again, the addition of a heat pump increases the possible operating points, although the exergy efficiency reduces (at some points, up to 50% of the original value).
- In terms of primary energy, all studied configurations can have energy savings (between 20 and 60%), depending on the efficiency of hydrogen production pathway. But also, in all configurations there are operating conditions at which primary energy losses appear. Then, it is very important to match the power of the FC-mCHP to the demand characteristics (defined by the mean electrical power and the heat to power ratio).
- In general, there are always CO2 emissions savings compared with the reference configuration. These savings can be of about 50% for configurations with hydrogen production by SMR but without CO2 capture (C1 and C2), and as high as 300% for configurations with SMR combined with CO2 capture (C3) or electrolysis CO2-free configurations (C4 and C5). The parameters that most determine the results are the CO2 emissions factor of the hydrogen production configuration and the excess electrical energy generated by the FC-mCHP that can be fed-in into the grid.
- CO2 savings can be even higher when the operating strategy is satisfying thermal demand (up to 400% for C3 and C5). This is a consequence of the induced CO2 savings due to the avoidance of conventional electricity production, substituted by the electricity generated in excess by the FC-mCHP system and fed-in into the grid.
- As for the economic analysis, all configurations lead to negative savings (losses) compared to the reference configuration. The results are very sensitive to the operating conditions, in addition to the hydrogen cost and the investment costs. The trends of economic savings are the opposite of CO2 emissions savings, showing the trade-off between both results.

Further research can be proposed from the results of this work. The model already developed can be used for more specific studies within each configuration. It could be also interesting to extend the model to consider thermal storage, cooling systems and new renewable energy generation systems such as solar energy.

CRediT authorship contribution statement

P. Gabana: Software, Methodology, Investigation, Formal analysis, Conceptualization, Writing – original draft. **M. Reyes:** Writing – review & editing, Validation, Resources. **F.V. Tinaut:** Writing – original draft, Resources, Project administration, Conceptualization. **R. Novella:** Writing – review & editing, Visualization, Supervision, Project administration.

Declaration of competing interest

The authors declare that they have no known competing financial interests or personal relationships that could have appeared to influence the work reported in this paper.

Acknowledgements

This work has been developed as a collaboration between the research groups Thermal Engines and Renewable Energies (MyER) group (University of Valladolid-UVa) and Institute CMT (Universitat Politècnica de València-UPV).

Pedro Gabana Molina has been awarded a predoctoral contract UVa-Bank of Santander in the 2021 call.

Appendix 1

This appendix includes the expressions that relate the main performance variables of the FC-mCHP system, including the hydrogen production phase and the possibility of combining with a heat pump. The subsystems and the energy flows were presented in Fig. 4 of the main text.

For a clearer explanation, some expressions already introduced in the main body of the paper are repeated here. The mean annual energy efficiencies (electrical, thermal and global) of the FC-mCHP system are defined according to Eqs. (19)–(21):

$$\eta_{el,FC} = \frac{E_{el,FC}}{E_{H2,FC}} \tag{19}$$

$$\eta_{th,FC} = \frac{E_{th,FC}}{E_{H2,FC}} \tag{20}$$

$$\eta_{gl,FC} = \eta_{el,FC} + \eta_{th,FC} = \frac{E_{el,FC} + E_{th,FC}}{E_{H2,FC}} \tag{21}$$

With the adopted definition, this mean annual energy global efficiency of just the FC-mCHP is always less than unity.

Accounting for the hydrogen production processes plus the possible combination with a heat pump leads to similar expressions of the annual electrical and thermal efficiencies but considering as reference the amount of primary energy required to generate the hydrogen that feeds the FC-mCHP, Eqs. (22) and (23). In the case of thermal energy, the term χ appearing in Eq. (23) is called energy ratio instead of thermal efficiency since the term corresponding to the heat taken from environment (E_{th_0} in Fig. 4 of the main text) is not considered in the denominator of the expression and under certain conditions the energy ratio χ can be higher than unity.

$$\eta_{el,FC+HP} = \frac{E_{el,FC}}{E_{H2,Prim}} \tag{22}$$

$$\chi_{th,FC+HP} = \frac{E_{th,FC} + E_{th,HP}}{E_{H2,Prim}} \tag{23}$$

The exergy associated to the hydrogen flow is related to the energy associated to the hydrogen flow by means of a characteristic factor φ_{H2} which depends on the fuel composition (although its value for hydrogen is very close to 1, 0.985 [69]), according to Eq. (24):

$$Ex_{H2} = \varphi_{H2} \bullet E_{H2} \tag{24}$$

This relationship helps to express the exergy efficiencies in terms of the energy efficiencies. For instance, the mean annual electrical exergy efficiency is equal to the electrical energy efficiency multiplied by the inverse of φ_{H2}:

$$\eta_{Ex,el,FC} = \frac{Ex_{el,FC}}{Ex_{H2,FC}} = \frac{1}{\varphi_{H2}}\eta_{el,FC} \tag{25}$$

All thermal energies are generated at a characteristic temperature that defines their exergy content. Then the mean annual thermal exergy efficiency is equal to the thermal energy efficiency multiplied by the Carnot factor corresponding to the hot temperature sink (Eq. (26)):

$$\eta_{Ex,th,FC} = \frac{Ex\left(E_{th,FC}\right)}{Ex_{H2,FC}} = \frac{1}{\varphi_{H2}}\eta_{th,FC}\left(1 - \frac{T_0}{T_{th,FC}}\right) \tag{26}$$

When a heat pump is added to the system, FC-mCHP + HP, it is possible to use part of the electrical energy generated by the FC-mCHP to pump heat taken from environment (E_{th_0}) up to the temperature level required by the demand. The total thermal energy pumped is calculated from the electric energy input with a multiplicative effect given by the heat pump CoP (Eq. (27)):

$$E_{th,HP} = E_{el,HP} * CoP = \left(E_{el,FC} - E_{el,D}\right) * CoP \tag{27}$$

The exergy efficiency of the heat pump can be expressed using its CoP and the Carnot efficiency (Eq. (28)):

$$\eta_{Ex,HP} = \frac{Ex\left(E_{th,HP}\right)}{Ex_{el,HP}} = \frac{E_{th,HP}}{E_{el,HP}}\left(1 - \frac{T_0}{T_{th,HP}}\right) = CoP\left(1 - \frac{T_0}{T_{th,HP}}\right) \tag{28}$$

The Heat to Power Ratio of the combined FC-mCHP + HP system is defined according to Eq. (29).

$$HPR_{FC+HP} = \frac{E_{th,FC} + E_{th,HP}}{E_{el,FC} - E_{el,HP}} \tag{29}$$

If the heat pump does not work, $E_{el,HP} = E_{th,HP} = 0$ and the system reduces to a FC-mCHP alone, with a HPR_{FC} given by Eq. (30).

$$HPR_{FC} = \frac{E_{th,FC}}{E_{el,FC}} \tag{30}$$

According to the operation mode of the combined FC-mCHP + HP system, the electrical energy produced by the FC-mCHP has to cover the electrical energy demanded and the electrical energy needed by the heat pump (Eq. (31)).

$$E_{el,FC} = E_{el,D} + E_{el,HP} = E_{el,D} + \frac{E_{th,HP}}{CoP} \tag{31}$$

The parameter β_{HP} is introduced to quantify the fraction of electrical energy produced by the FC-mCHP that is used to drive the heat pump (Eq. (32)):

$$\beta_{HP} = \frac{E_{el,HP}}{E_{el,FC}} \tag{32}$$

If $\beta_{HP} = 0$ only the FC-mCHP works, while if $\beta_{HP} = 1$ all electrical energy produced by the fuel cell is used to drive the heat pump, with no electrical energy available to satisfy electrical demand (and then $HPR_{FC+HP} \rightarrow \infty$).

Considering the parameter β_{HP}, the resulting HPR_{FC+HP} expression is Eq. (33).

$$HPR_{FC+HP} = \frac{E_{th,FC} + E_{th,HP}}{E_{el,FC} - E_{el,HP}} = \frac{\frac{E_{th,FC}}{E_{el,FC}} + \frac{E_{th,HP}}{E_{el,FC}}}{1 - \frac{1}{CoP}\frac{E_{th,HP}}{E_{el,FC}}} = \frac{HPR_{FC} + \frac{E_{th,HP}}{E_{el,FC}}}{1 - \frac{E_{el,HP}}{E_{el,FC}}} = \frac{HPR_{FC} + \frac{E_{el,HP} \bullet CoP}{E_{el,FC}}}{1 - \frac{E_{el,HP}}{E_{el,FC}}} = \frac{HPR_{FC} + \beta_{HP} \bullet CoP}{1 - \beta_{HP}} \tag{33}$$

In Fig. 1 the dependence of HPR_{FC+HP} on the parameter β_{HP} is plotted considering two sets of values of CoP and HPR_{FC}.

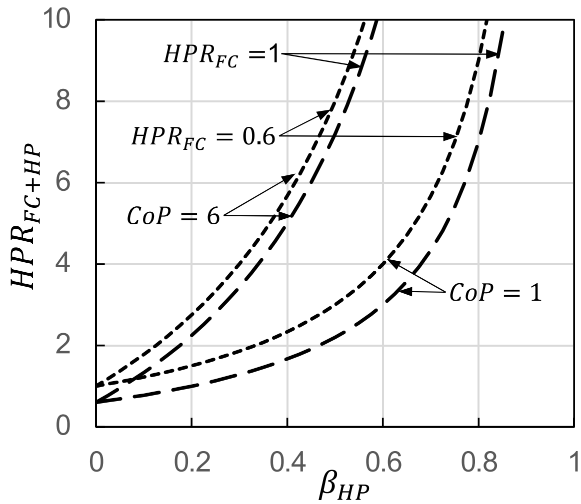

Fig. 1. Dependence of HPR of combined system FC-mCHP + HP on β_{HP}.

The mean annual global energy ratio of the FC-mCHP + HP system, from hydrogen energy to electric and thermal energies produced, can be expressed including the parameter β_{HP} as Eq. (34):

$$\chi_{gl,FC+HP} = \frac{E_{el,D} + E_{th,FC} + E_{th,HP}}{E_{H2}} = \frac{E_{el,D}}{E_{H2}} + \eta_{th,FC} + \frac{E_{th,HP}}{E_{H2}} = \eta_{el,FC} - \frac{E_{el,HP}}{E_{H2}} + \eta_{th,FC} + \frac{CoP \bullet E_{el,HP}}{E_{H2}} = \eta_{el,FC} + \eta_{th,FC} + \frac{E_{el,HP}}{E_{H2}}(CoP-1) = \eta_{el,FC} + \eta_{th,FC} + \beta_{HP} \bullet \frac{E_{el,FC}}{E_{H2}}(CoP-1) = \eta_{th,FC} + \eta_{el,FC}\,(1+\beta_{HP}(CoP-1)) = \eta_{el,FC}[1 + HPR_{FC} + \beta_{HP}(CoP-1)] \tag{34}$$

If the primary energy required to generate the hydrogen is considered as reference for the global efficiency, an expression formally identical to Eq. (34) is obtained, with the only difference that the electrical efficiency from primary energy given by Eq. (22) must be used.

The mean annual global energy ratio given by Eq. (34) considers only as input the hydrogen energy. However, heat is also taken from ambient as an input to the heat pump. For that reason, this mean annual global energy ratio χ can have values higher than unity in some conditions.

The mean annual exergy efficiency of the FC-mCHP + HP system follows Eq. (35):

$$\eta_{Ex,FC+HP} = \frac{E_{el,D} + E_{th,FC}\left(1-\frac{T_0}{T_{th,FC}}\right) + E_{th,HP}\left(1-\frac{T_0}{T_{th,HP}}\right)}{\varphi_{H2} \bullet E_{H2}} = \frac{1}{\varphi_{H2}}\left[\frac{E_{el,FC} - E_{el,HP} + E_{th,FC}\left(1-\frac{T_0}{T_{th,FC}}\right) + E_{th,HP}\left(1-\frac{T_0}{T_{th,HP}}\right)}{E_{H2}}\right] = \frac{1}{\varphi_{H2}}\left[\eta_{el,FC} - \beta_{HP} \bullet \eta_{el,FC} + \eta_{th,FC}\left(1-\frac{T_0}{T_{th,FC}}\right) + \beta_{HP} \bullet \eta_{el,FC} \bullet CoP\left(1-\frac{T_0}{T_{th,HP}}\right)\right] = \frac{1}{\varphi_{H2}}\left[\eta_{th,FC}\left(1-\frac{T_0}{T_{th,FC}}\right) + \eta_{el,FC} \bullet \left(1+\beta_{HP} \bullet \left(CoP\left(1-\frac{T_0}{T_{th,HP}}\right)-1\right)\right)\right] = \frac{\eta_{el,FC}}{\varphi_{H2}}\left[1 + HPR_{FC}\left(1-\frac{T_0}{T_{th,FC}}\right) + \beta_{HP} \bullet \left(CoP\left(1-\frac{T_0}{T_{th,HP}}\right)-1\right)\right] \tag{35}$$

Even though the heat taken from ambient as input to the heat pump E_{th_0} is not explicitly considered in the denominator of Eq. (35) of the global exergy efficiency, its associated exergy is always zero (since its characteristic temperature is the ambient temperature). As a result, the global exergy efficiency given by Eq. (35) has always values less than unity. As before, the extension to consider the efficiency from primary energy is immediate, just by introducing the associated electrical efficiency from primary energy given by Eq. (22).

Finally, the ratio between the mean annual exergy efficiency and the global energy ratio of the FC-mCHP + HP system is given by Eq. (36):

$$\frac{\eta_{Ex,FC+HP}}{\chi_{gl,FC+HP}} = \frac{1}{\varphi_{H2}} \frac{1 + HPR_{FC}\left(1-\frac{T_0}{T_{th,FC}}\right) + \beta_{HP} \bullet \left[CoP\left(1-\frac{T_0}{T_{th,HP}}\right)-1\right]}{1 + HPR_{FC} + \beta_{HP}(CoP-1)} \tag{36}$$

Appendix 2

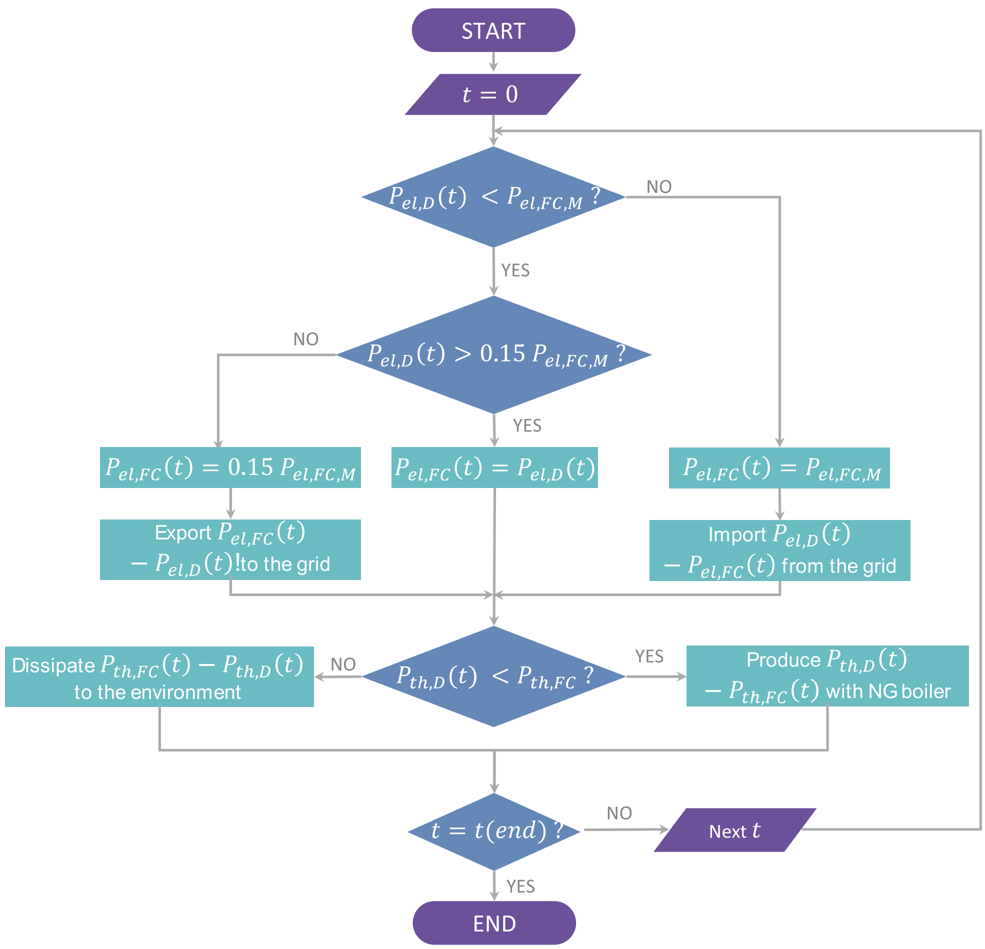

Fig. 2. Flowchart of the operation strategy adopted by the FC-mCHP to meet electrical demand D_{el}.

Appendix 3

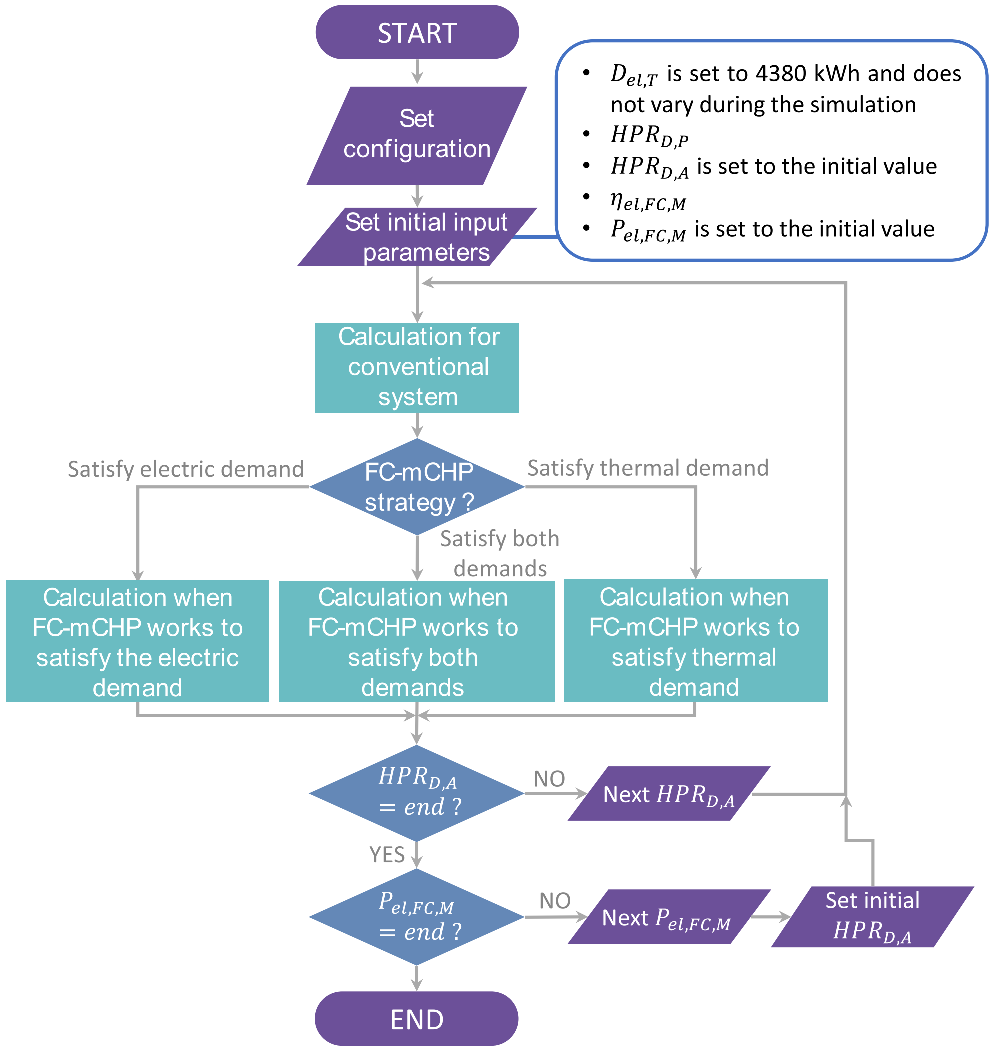

Fig. 3. Flowchart of program operation.

References

[1] Maghanki MM, Ghobadian B, Najafi G, Galogah RJ. Micro combined heat and power (MCHP) technologies and applications. Renew Sustain Energy Rev 2013;28:510–24. https://doi.org/10.1016/j.rser.2013.07.053.

[2] Murugan S, Horák B. A review of micro combined heat and power systems for residential applications. Renew Sustain Energy Rev 2016;64:144–62. https://doi.org/10.1016/j.rser.2016.04.064.

[3] Martinez S, Michaux G, Salagnac P, Bouvier J-L. Micro-combined heat and power systems (micro-CHP) based on renewable energy sources. Energy Convers Manag 2017;154:262–85. https://doi.org/10.1016/j.enconman.2017.10.035.

[4] Dentice d'Accadia M, Sasso M, Sibilio S, Vanoli L. Micro-combined heat and power in residential and light commercial applications. Appl Therm Eng 2003;23:1247–59. https://doi.org/10.1016/S1359-4311(03)00030-9.

[5] Hawkes A, Staffell I, Brett D, Brandon N. Fuel cells for micro-combined heat and power generation. Energy Environ Sci 2009;2:729. https://doi.org/10.1039/b902222h.

[6] Barelli L, Bidini G, Gallorini F, Ottaviano A. Dynamic analysis of PEMFC-based CHP systems for domestic application. Appl Energy 2012;91:13–28. https://doi.org/10.1016/j.apenergy.2011.09.008.

[7] Hwang JJ, Zou ML. Development of a proton exchange membrane fuel cell cogeneration system. J Power Sources 2010;195:2579–85. https://doi.org/10.1016/j.jpowsour.2009.10.087.

[8] Romdhane J, Louahlia-Gualous H. Energy assessment of PEMFC based MCCHP with absorption chiller for small scale French residential application. Int J Hydrogen Energy 2018;43:19661–80. https://doi.org/10.1016/j.ijhydene.2018.08.132.

[9] Adam A, Fraga ES, Brett DJL. Options for residential building services design using fuel cell based micro-CHP and the potential for heat integration. Appl Energy 2015;138:685–94. https://doi.org/10.1016/j.apenergy.2014.11.005.

[10] Di Marcoberardino G, Roses L, Manzolini G. Technical assessment of a micro-cogeneration system based on polymer electrolyte membrane fuel cell and fluidized bed autothermal reformer. Appl Energy 2016;162:231–44. https://doi.org/10.1016/j.apenergy.2015.10.068.

[11] Martínez Reverte I, Gómez-Navarro T, Sánchez-Díaz C, Montagud Montalvá C. Evaluation of alternatives for energy supply from fuel cells in compact cities in the mediterranean climate; case study: city of valencia. Energies 2022;15:4502. https://doi.org/10.3390/en15124502.

[12] Gandiglio M, Ferrero D, Lanzini A, Santarelli M. Fuel cell cogeneration for building sector: European status. https://www.rehva.eu/rehva-journal/chapter/default-2ec3ec3581; 2020.

[13] Xie D, Wang Z, Jin L, Zhang Y. Energy and exergy analysis of a fuel cell based micro combined heat and power cogeneration system. Energy Build 2012;50:266–72. https://doi.org/10.1016/j.enbuild.2012.03.047.

[14] Napoli R, Gandiglio M, Lanzini A, Santarelli M. Techno-economic analysis of PEMFC and SOFC micro-CHP fuel cell systems for the residential sector. Energy Build 2015;103:131–46. https://doi.org/10.1016/j.enbuild.2015.06.052.

[15] Gandiglio M, Lanzini A, Santarelli M, Leone P. Design and optimization of a proton exchange membrane fuel cell CHP system for residential use. Energy Build 2014;69:381–93. https://doi.org/10.1016/j.enbuild.2013.11.022.

[16] Sorace M, Gandiglio M, Santarelli M. Modeling and techno-economic analysis of the integration of a FC-based micro-CHP system for residential application with a

heat pump. Energy 2017;120:262–75. https://doi.org/10.1016/j.energy.2016.11.082.
[17] Chang H, Duan C, Xu X, Pei H, Shu S, Tu Z. Technical performance analysis of a micro-combined cooling, heating and power system based on solar energy and high temperature PEMFC. Int J Hydrogen Energy 2019;44:21080–9. https://doi.org/10.1016/j.ijhydene.2018.11.217.
[18] Atienza-Márquez A, Bruno JC, Coronas A. Potential uses of the heat released in hydrogen fuel cells: overview and case-study analysis. In: European hydrogen energy conference; 2022.
[19] Chahartaghi M, Kharkeshi BA. Performance analysis of a combined cooling, heating and power system with PEM fuel cell as a prime mover. Appl Therm Eng 2018;128:805–17. https://doi.org/10.1016/j.applthermaleng.2017.09.072.
[20] Elmamoun S, El Maakoul A, Bouhssine Z, Bouramdane A-A, Degiovanni A. Performance analysis of a fuel cell-based combined heating, cooling, and power system for a residential building: a case study in Morocco. Energy Convers Manag 2024;321:119067. https://doi.org/10.1016/j.enconman.2024.119067.
[21] Xie P, Zhou F, Tan S, Liso V, Sahlin SL. Development of a two-layer control and management system for a residential microgrid with HT-PEMFC-based micro-CHP. Appl Energy 2025;381:125118. https://doi.org/10.1016/j.apenergy.2024.125118.
[22] Byun J, Go J, Kim C, Heo Y. Reliability, economic, and environmental analysis of fuel-cell-based hybrid renewable energy networks for residential communities. Energy Convers Manag 2023;284:116964. https://doi.org/10.1016/j.enconman.2023.116964.
[23] Chen JMP, Ni M. Economic analysis of a solid oxide fuel cell cogeneration/trigeneration system for hotels in Hong Kong. Energy Build 2014;75:160–9. https://doi.org/10.1016/j.enbuild.2014.01.053.
[24] Mottaghizadeh P, Jabbari F, Brouwer J. Integrated solid oxide fuel cell, solar PV, and battery storage system to achieve zero net energy residential nanogrid in California. Appl Energy 2022;323:119577. https://doi.org/10.1016/j.apenergy.2022.119577.
[25] Hawkes A, Leach M. Cost-effective operating strategy for residential micro-combined heat and power. Energy 2007;32:711–23. https://doi.org/10.1016/j.energy.2006.06.001.
[26] Wang Y, Zeng Z, Wang T, Che Z. Dynamic simulation and optimization of a residential proton exchange membrane fuel cell (PEMFC) combined heat and power (CHP) system. Energy 2025;319:134865. https://doi.org/10.1016/j.energy.2025.134865.
[27] Arsalis A. A comprehensive review of fuel cell-based micro-combined-heat-and-power systems. Renew Sustain Energy Rev 2019;105:391–414. https://doi.org/10.1016/j.rser.2019.02.013.
[28] Gabana P, Tinaut FV, Reyes M, Domínguez JI. Performance evaluation of a fuel cell mCHP system under different configurations of hydrogen origin and heat recovery. Energies 2023;16:6420. https://doi.org/10.3390/en16186420.
[29] Facci AL, Ubertini S. Analysis of a fuel cell combined heat and power plant under realistic smart management scenarios. Appl Energy 2018;216:60–72. https://doi.org/10.1016/j.apenergy.2018.02.054.
[30] Kayfeci M, Keçebaş A, Bayat M. Hydrogen production. In: Solar hydrogen production. Elsevier; 2019. p. 45–83. https://doi.org/10.1016/B978-0-12-814853-2.00003-5.
[31] Dawood F, Anda M, Shafiullah GM. Hydrogen production for energy: an overview. Int J Hydrogen Energy 2020;45:3847–69. https://doi.org/10.1016/j.ijhydene.2019.12.059.
[32] Motapon SN, Tremblay O, Dessaint LA. Development of a generic fuel cell model: application to a fuel cell vehicle simulation. Int J Power Electron 2012;4:505. https://doi.org/10.1504/IJPELEC.2012.052427.
[33] Barbir F. PEM fuel cells. second ed. Academic Press; 2012.
[34] Budak Y, Devrim Y. Investigation of micro-combined heat and power application of PEM fuel cell systems. Energy Convers Manag 2018;160:486–94. https://doi.org/10.1016/j.enconman.2018.01.077.
[35] Dutta S, Shimpalee S, Van Zee JW. Numerical prediction of mass-exchange between cathode and anode channels in a PEM fuel cell. Int J Heat Mass Tran 2001;44:2029–42. https://doi.org/10.1016/S0017-9310(00)00257-X.
[36] Dannenberg K, Ekdunge P, Lindbergh G. Mathematical model of the PEMFC. J Appl Electrochem 2000;30:1377–87. https://doi.org/10.1023/A:1026534931174.
[37] Ge S-H, Yi B-L. A mathematical model for PEMFC in different flow modes. J Power Sources 2003;124:1–11. https://doi.org/10.1016/S0378-7753(03)00584-6.
[38] Nazari-Heris M, Abapour S, Mohammadi-Ivatloo B. Optimal economic dispatch of FC-CHP based heat and power micro-grids. Appl Therm Eng 2017;114:756–69. https://doi.org/10.1016/j.applthermaleng.2016.12.016.
[39] Wakui T, Wada N, Yokoyama R. Energy-saving effect of a residential polymer electrolyte fuel cell cogeneration system combined with a plug-in hybrid electric vehicle. Energy Convers Manag 2014;77:40–51. https://doi.org/10.1016/j.enconman.2013.09.018.
[40] Chen X, Zhou H, Li W, Yu Z, Gong G, Yan Y, Luo L, Wan Z, Ding Y. Multi-criteria assessment and optimization study on 5 kW PEMFC based residential CCHP system. Energy Convers Manag 2018;160:384–95. https://doi.org/10.1016/j.enconman.2018.01.050.
[41] Xu Y, Luo X, Tu Z. Siew Hwa Chan, Multi-criteria assessment of solid oxide fuel cell–combined cooling, heating, and power system model for residential application. Energy 2022;259:124974. https://doi.org/10.1016/j.energy.2022.124974.
[42] Peacock AD, Newborough M. Impact of micro-CHP systems on domestic sector CO2 emissions. Appl Therm Eng 2005;25:2653–76. https://doi.org/10.1016/j.applthermaleng.2005.03.015.
[43] Cappa F, Facci AL, Ubertini S. Proton exchange membrane fuel cell for cooperating households: a convenient combined heat and power solution for residential applications. Energy 2015;90:1229–38. https://doi.org/10.1016/j.energy.2015.06.092.
[44] Hawkes A, Leach M. Impacts of temporal precision in optimisation modelling of micro-Combined Heat and Power. Energy 2005;30:1759–79. https://doi.org/10.1016/j.energy.2004.11.012.
[45] Red Eléctrica Española, (n.d.). https://www.ree.es/es/clientes/generador/gestion-medidas-electricas/consulta-perfiles-de-consumo.
[46] Previsión de demanda ENAGAS, Https://Www.Enagas.Es/Es/Gestion-Tecnica-Sistema/Energy-Data/Demanda/Prevision/[n.d.)].
[47] Proton Motor, (n.d.). https://www.proton-motor.de/en/products/fuel-cell-stacks/.
[48] Pohl E, Meier P, Maximini M, vom Schloß J. Primary energy savings of a modular combined heat and power plant based on high temperature proton exchange membrane fuel cells. Appl Therm Eng 2016;104:54–63. https://doi.org/10.1016/j.applthermaleng.2016.05.055.
[49] Meggers F, Leibundgut H. The potential of wastewater heat and exergy: decentralized high-temperature recovery with a heat pump. Energy Build 2011;43:879–86. https://doi.org/10.1016/j.enbuild.2010.12.008.
[50] Temperature of different places in europe. https://thingspeak.com/channels/143789; 2022.
[51] Hervas Estefania, Marchante Javier, Navarro-Peris Emilio, Corberan Jose Miguel. Design of a system for the production of domestic hot water from wastewater heat recovery based on a heat pump optimized to work at high water temperature lif. In: International high performance buildings conference, purdue e-pubs. Purdue University; 2018.
[52] X. Masip, Lucas Álvarez-Piñeiro, Estefanía Hervas-Blasco, Emilio Navarro-Peris, J. M. Corberán, Heat Pump control comparison of a conventional superheat system over a subcooling control system for Domestic Hot Water production, in: XI national and II international engineering thermodynamics congress, n.d.
[53] U.S. Energy Information Administration (EIA), How much electricity is lost in electricity transmission and distribution in the United States?, (n.d.). https://www.eia.gov/tools/faqs/faq.php?id=105&t=3 (accessed August 9, 2023).
[54] Selectra, Factura de la luz: desglose y explicación de conceptos. https://selectra.es/energia/info/que-es/factura-luz. [Accessed 9 August 2023].
[55] Selectra. Precio del gas natural: Evolución en España y coste del m3. https://selectra.es/energia/info/que-es/precio-kwh-gas-natural. [Accessed 9 August 2023].
[56] SENDECO2, Precios CO2 , (n.d.). https://www.sendeco2.com/es/precios-co2 (accessed August 9, 2023).
[57] 2022 U.S. electricity flow, U.S. electricity flow. https://www.eia.gov/totalenergy/data/flow-graphs/electricity.php. [Accessed 9 August 2023].
[58] Che D, Liu Y, Gao C. Evaluation of retrofitting a conventional natural gas fired boiler into a condensing boiler. Energy Convers Manag 2004;45:3251–66. https://doi.org/10.1016/j.enconman.2004.01.004.
[59] The Future of Hydrogen Seizing today's opportunities. https://www.iea.org/reports/the-future-of-hydrogen. [Accessed 9 August 2023].
[60] Staffell I, Green R. The cost of domestic fuel cell micro-CHP systems. Int J Hydrogen Energy 2013;38:1088–102. https://doi.org/10.1016/j.ijhydene.2012.10.090.
[61] Selectra, ¿Cuál es el precio de los excedentes de autoconsumo hoy en PVPC?. https://selectra.es/autoconsumo/info/tarifas/pvpc#esios-precio-excedentes-autoconsumo. [Accessed 9 August 2023].
[62] Barati M, Esfahani S, Utigard TA. Energy recovery from high temperature slags. Energy 2011;36:5440–9. https://doi.org/10.1016/j.energy.2011.07.007.
[63] Argus hydrogen and future fuels. Https://Www.Argusmedia.Com/En/Solutions/Products/Argus-Hydrogen-and-Future-Fuels; 2024.
[64] Fakheri A. Efficiency analysis of heat exchangers and heat exchanger networks. Int J Heat Mass Tran 2014;76:99–104. https://doi.org/10.1016/j.ijheatmasstransfer.2014.04.027.
[65] Selectra, Compañías de energía verde en España: listado y comparativa (2023). https://climate.selectra.com/es/companias-energia-verde. [Accessed 9 August 2023].
[66] Hakkaki-Fard A, Eslami-Nejad P, Aidoun Z, Ouzzane M. A techno-economic comparison of a direct expansion ground-source and an air-source heat pump system in Canadian cold climates. Energy 2015;87:49–59. https://doi.org/10.1016/j.energy.2015.04.093.
[67] Kilpatrick RAR, Banfill PFG, Jenkins DP. Methodology for characterising domestic electrical demand by usage categories. Appl Energy 2011;88:612–21. https://doi.org/10.1016/j.apenergy.2010.08.002.
[68] Bianchi M, De Pascale A, Spina PR. Guidelines for residential micro-CHP systems design. Appl Energy 2012;97:673–85. https://doi.org/10.1016/j.apenergy.2011.11.023.
[69] Kotas TJ. The exergy method of thermal plant analysis. Elsevier; 1985. https://doi.org/10.1016/C2013-0-00894-8.